NAVAL FACILITIES ENGINEERING SERVICE CENTER
Port Hueneme, California 93043-4370

Technical Memorandum
TM-2276-AMP

MEASUREMENT OF TRANSIENT FLOW INDUCED BY A BERTHING BARGE

by

E.T. Huang
D.A. Davis
C.H. Kim
H.C. Chen

March 1998

Sponsored by
Office of Naval Research
Arlington, VA 22217-5660

REPORT DOCUMENTATION PAGE

Form Approved
OMB No. 0704-018

1. AGENCY USE ONLY *(Leave blank)*	2. REPORT DATE	3. REPORT TYPE AND DATES COVERED
	March 1998	Final; FY97

4. TITLE AND SUBTITLE

MEASUREMENT OF TRANSIENT FLOW INDUCED BY A BERTHING BARGE

5. FUNDING NUMBERS

6. AUTHOR(S)

E.T. Huang, D.A. Davis, C.H. Kim,* and H.C. Chen*
*Texas A&M University

7. PERFORMING ORGANIZATION NAME(S) AND ADDRESSE(S)

Naval Facilities Engineering Service Center
1100 23rd Ave.
Port Hueneme, CA 93043-4370

8. PERFORMING ORGANIZATION REPORT NUMBER

TM-2276-AMP

9. SPONSORING/MONITORING AGENCY NAME(S) AND ADDRESSES

Office of Naval Research
Arlington, VA 22217-5660

10. SPONSORING/MONITORING AGENCY REPORT NUMBER

11. SUPPLEMENTARY NOTES

12a. DISTRIBUTION/AVAILABILITY STATEMENT

Approved for public release; distribution is unlimited.

12b. DISTRIBUTION CODE

13. ABSTRACT *(Maximum 200 words)*

The Navy is developing a numerical solution that uses the Chimera RANS/free-surface technique to address the critical features of transient flow around a berthing ship. Experimental data required to validate the ship berthing model were collected during scale model tests conducted at a shallow water model basin. The test setup included a towing carriage traveling on rail guides used to power a scale model barge toward the modeled quay wall. The test matrix included three different values of water depth, approach speed, and approach angle. Acoustic doppler velocity meters were used to measure water particle velocity. The scale model barge was found to draw a significant volume of water behind, and push a measurable volume before, as it approached the quay wall.

14. SUBJECT TERMS

Ship berthing, fender design, hydrodynamic coupling, Chimera RANS/free-surface technique

15. NUMBER OF PAGES

45

16. PRICE CODE

17. SECURITY CLASSIFICATION OF REPORT	18. SECURITY CLASSIFICATION OF THIS PAGE	19. SECURITY CLASSIFICATION OF ABSTRACT	
Unclassified	Unclassified	Unclassified	UL

EXECUTIVE SUMMARY

A test program was conducted at a shallow water model basin to collect essential experimental data required to validate a realistic ship berthing model being developed for the Navy. The new computational technique will be used to upgrade currently accepted analytical fender design procedures that rely on constant-value added-mass coefficients to account for hydrodynamic coupling effects between the vessel, quay wall, and the ambient watercourse. Fenders designed in this manner tend to either be underdesigned, resulting in a high rate of failure, or overdesigned, producing a more costly product.

The Chimera RANS/free-surface technique being developed is a numerical solution capable of addressing critical features of transient flow around a berthing ship. Features of the simulation model include underkeel flow acceleration, separation around the bow and stern, flow recirculation behind the ship, water cushioning effects between ship and quay wall, and complex interaction among bow, shoulder, and stern wave systems. Validating experiments were conducted in a basin 26 meters long, 9.8 meters wide, and 0.76 meter deep, in which water depth could be adjusted to accommodate a range of desired underkeel-clearance-to-vessel-draft ratios. The test setup included a towing carriage traveling on guide rails used to power a scale model barge toward the modeled quay wall. A pair of coil springs mounted on the quay wall simulated the fender system. Individual test runs were completed by stopping the forward travel of the barge just short of the quay wall.

The test matrix included three values of water depth, three values of approach speed, and three values of approach angle. The general flow of water at the free surface was established using floating ping-pong balls to trace movement, while flow patterns at the bottom of the tank were established using neutrally buoyant beads. Three acoustic doppler velocity meters, one a permanent three-dimensional gauge (affixed to the barge) and the others removable two-dimensional gauges, were used to measure water particle velocity. Each test was repeated three times for a set of given parameters so that the two-dimensional gauges could be relocated, providing results for a total of six observation sites.

It was found that a particular test could be repeated reasonably well even though it was not possible to duplicate the precise history of carriage movement from run to run. In all of the test runs, the scale model barge was found to draw a significant volume of trailing water behind as it approached the quay wall. The movement of trailing water persisted even after the barge came to an abrupt stop. The barge also pushed a substantial volume of water in front, but the distance influenced seemed to be less than the distance of trailing water. On the underside of the barge model, fluid directly under the keel was drawn forward at the start of a run due to viscosity effects. With continued movement forward, some of the fluid displaced in front was pushed back under the keel, causing a back flow condition that increased with continued movement ahead. When the barge came to a sudden stop just in front of the quay wall, the trailing mass of fluid continued forward, pushing its way through the underkeel clearance, resulting in another reversal of flow direction. This positive direction of flow which continued to push the back of the barge accounted for the so-called "added mass" effect which is a well known phenomenon in ship berthing practice.

A number of additional findings and observations relating to flow patterns and reversal of flow are included in the remarks section of this report. The model basin tests produced excellent

comparisons between flow patterns measured during the "deep" water series of tests and water currents predicted by the simulation model. The large volume of water trailing the barge was shown to contribute significantly to the resulting berthing energy, especially in those runs where water depth was small compared to ship draft.

CONTENTS

INTRODUCTION

Objective

The U.S. Navy is currently developing methods to accurately predict the forces imposed on a pier or wharf fender system during the berthing of a ship (Ref 1). The primary objective of this experimental effort has been to acquire the essential engineering data necessary to validate a high precision simulation model – a model that quantifies the amount of energy passed from a ship and ambient water to a fender system as the vessel is berthed. The new computational technique will be used to upgrade fender design procedures cited in MIL-HDBK-1025/1 (Ref 2).

Background

Damage due to berthing can result in substantial financial and operational penalties to ships and wharves. Even in a well executed berthing operation, the kinetic energy of a large ship is sufficient to seriously damage a berthing structure whenever the protective fender system is not properly sized and configured to absorb and dissipate kinetic energy progressively, mitigating the effects of sudden impact forces. The amount of energy absorbed and the maximum impact force imparted are the primary criteria applied in accepted fender design practices. However, because berthing is a highly complex process that includes structural and fluid coupling between a vessel, a fender system, and the surrounding water, a reliable and accredited assessment tool for computing berthing energy has not been developed. Currently, most accepted fender design methods account for the influence of the ambient water by using a simple constant coefficient. Fenders designed this way tend to be either underdesigned, resulting in a high rate of failure, or overdesigned, producing a more costly product.

In order to improve the design of a fender system, it is mandatory that the analytical techniques include an accurate hydrodynamic model for simulating ambient flow activities during a typical vessel approach to a berthing structure. The model must simulate the effects of fluid viscosity, water cushioning, and free-surface variation to accurately predict the hydrodynamic coupling that takes place between the vessel and the berthing structure.

Current design procedures use one or more of the following types of data to determine the desired maximum energy absorbing capacity of a structure: empirical, statistical, or analytical. The first two methods require an interpretation of the statistical data base of berthing energy measurements. Strictly speaking, these two methods are limited to the particular hull forms, sites, and berthing scenarios addressed by the data base. Establishing an extensive data base is expensive and labor intensive. The analytical method relates the berthing energy directly to the kinetic energy of the ship at the moment the vessel impacts a fender structure. The current design practice uses a series of correcting factors to account for the influence of ambient water, residual ship dynamics, ship hull elasticity, and fender structure configuration. This relation may be represented by the following equation:

$$E_f = E_s \bullet C_e \bullet C_m \bullet C_s \bullet C_c$$

$$E_s = \frac{1}{2} m_s U^2$$

where

E_f = energy to be absorbed by the fender
E_s = energy of the approaching ship
U = the transverse speed of the ship
m_s = mass of the ship
C_e = eccentricity coefficient
C_m = hydrodynamic mass coefficient
C_s = softness coefficient of the fenders
C_c = berth configuration coefficient

Although this currently used analytical method is appealing because of its simplicity and adaptability to wide applications, it suffers from several deficiencies when put into design practice. The correction factors for ambient water effects, denoted as "added mass coefficients" for convenience, may vary widely from case to case. The uncertainty involved approaches an order of magnitude of the value to be assessed. In addition, it is intuitive that the hydrodynamic contribution of the transient flow induced by a berthing ship should be time varying and highly dependent on hull geometry, site configuration, and operational procedures, and as a result is not well represented by a constant correction factor. Because of these limitations, the fluid effect must be assessed for each specific case.

The Navy is currently developing a simulation model capable of addressing a realistic ship berthing process using a Chimera RANS/free-surface technique developed by Chen et al. (Ref 3) for the simulation of transient flow around a berthing ship. This analytical method solves the mean flow and turbulence quantities using arbitrary combinations of embedded, overlapped, or matched grids. The relative motion between various grid blocks is accommodated through the application of a Chimera domain decomposition technique. The numerical solution is capable of addressing critical features of transient flow around a berthing ship. These features include underkeel flow acceleration, separation around the bow and stern, flow recirculation behind the ship, water cushioning effects between ship and harbor quay wall, and the complex interaction among the bow, shoulder, and stern wave systems. This simulation model may be used to generate a broad data base covering a wide range of design parameters in support of practical design methodology. The test procedures described in this report were designed to validate the performance of the model developed by Chen.

TEST SETUP

A validation experiment was conducted at the shallow water model basin operated by the Civil Engineering Department at Texas A&M University, College Station, Texas. Figure 1 illustrates the general layout of the facility. The basin was 26 meters long, 9.8 meters wide, and 0.76 meter deep. The water depth was adjusted to provide a range of desired values of underkeel-clearance-to-vessel-draft ratio. The basin was equipped with a towing carriage that straddled the width of the basin and traveled on guide rails atop the side walls. The carriage was driven by a variable speed DC motor controlled by prescribed signals from a computer. About 7 meters at the western end of the basin were dedicated to an existing sand beach. At the eastern end, a vertically placed rectangular board made of plywood was secured to the bottom (near the idled wave generator) to represent a solid quay wall, as shown in Figure 2. A pair of coil springs was mounted on the quay wall to represent a fender system.

The working length of the test area from beach line to modeled quay wall was roughly 18 meters. A 1:8 scale model of the Navy's new pontoon barge was selected for the tests because of its inherent simple geometry, as illustrated in Figure 3. The barge model was 4.57 meters long, 0.95 meter wide, and 0.30 meter deep. The simple geometry of a barge structure was chosen for the purpose of producing the simple flow patterns that one would expect intuitively. The blunt shape of the hull also helped to amplify the hydrodynamic coupling effects between the vessel, quay wall, and seafloor. The test results using a simple geometry offered a better opportunity to emphasize the crucial flow features used to validate the numerical model.

The model was rigidly mounted near the center of the towing carriage, oriented parallel and lengthwise to the carriage. During the tests, the barge was towed sideways at constant speed toward the quay wall. Barge motion, including speed and excursion distance, was monitored using a potentiometer mounted on the quay wall, aligned amidship with the model. Movement of the towing carriage was also traced with a speed encoder, which provided a backup to the potentiometer readings. Three acoustic doppler velocity (ADV) meters, manufactured by Sontek of San Diego, California, were used to measure water particle velocity at selected sites. One meter was a three-dimensional (3D) gauge and the remaining two were two-dimensional (2D) gauges, used to accommodate the small clearance under the barge keel. Figure 4 shows the general features of a 3D gauge. The test gauges were calibrated by the manufacturer, and have a resolution of 0.1 mm/sec. The 3D ADV was mounted on the southern end of the model barge as shown in Figure 3. The 2D ADVs were either bolted to the basin floor or supported by thin rods at the midpoint of the water depth. The two 2D gauges were relocated to cover six different locations in a sequence of repeated tests of identical parameters.

Locations of the current meters are illustrated in Figure 5. A number of resistance-type wave gauges were employed to monitor changes at the free water surface. These gauges, however, were abandoned during the program because all changes in free surface elevation due to lateral barge motion were insignificantly small, sometimes smaller than the electronic noise introduced by carriage vibrations. All gauges were synchronized to a common clock during the tests and signals were relayed to a data acquisition computer.

The length of the barge at the waterline was 4.37 meters. The draft was maintained at 0.167 meter throughout the entire test program. The origin selected for the coordinate system was located on the free water surface, aligned with the center of the model barge at the start of a test run. The sign conventions for the axes were as follows: positive x-axis pointed in the

direction of barge motion, positive z-axis pointed up, and positive y-axis pointed in the direction necessary to complete a right-hand coordinate system. The coordinate system and the current meter locations are illustrated in Figure 5. Current meters C1 through C6 were fixed during each test run, while current meter C7 was free to move with the barge. The positional coordinates of the current meters are given in parenthesis in Figure 5.

TEST PROCEDURES

A test did not begin until measurable circulation in the basin had died out, and then it was conducted under continuous calm water conditions. At the start of a test, the model barge was positioned with its centerline aligned about 6.4 meters from the quay wall. The barge was accelerated to a constant velocity within 5 seconds of launch, and then continued at that velocity, stopping roughly 10 cm short of the quay wall. Data acquisition was initiated prior to the onset of barge motion in order to record the ambient condition. Time histories of barge excursion and water particle velocity were recorded simultaneously at a sampling rate of 8 hertz. Tests were repeated three times for a given set of parameters to allow rotation of the two 2D ADVs, providing results for a total of six current observation sites. Other parameters considered in a test included water depth, approach speed, and approach angle.

Water particle velocities were measured at various elevations. The water depth was set to 21, 26.7, and 35 cm, resulting in underkeel-clearance-to-vessel-draft ratios of 0.259, 0.599, and 1.096, respectively. Additional iterations of the test run were completed for approach speeds of 5, 10, and 20 cm/sec, and approach angles of 0, 5, and 10 degrees. Because of time constraints, the 5- and 10-degree approach angle tests were conducted at the 21-cm water depth. A complete test matrix is illustrated in Table 1.

The general flow pattern of water at the free surface was established using floating ping-pong balls to trace movement that was recorded by video camera, as shown in Figure 6. The flow pattern at the bottom of the tank was also traced during selected runs using neutrally buoyant beads. The submersed beads were deposited at three locations along the basin floor between the barge and the quay wall. Two deposits were located along the centerline of the basin, about 0.5 and 2 meters away from the quay wall, while the third deposit was located inside the north end of the barge, less than 1 meter from the quay wall.

TEST RESULTS

The acquisition system recorded extensive high frequency noise in all data channels, as shown in Figure 7. However, the data were successfully processed through a low pass filter to render a clearer trend of time history. Figure 8 gives a typical example of the filtered measurements. The thick dark line on the top chart indicates that the barge traveled approximately 6 meters in 65 seconds. The thin dark line and the gray line represent the barge speed as measured by the potentiometer and the speed encoder of the carriage, respectively. The two different velocity channels compared reasonably well for most passes, but in some recordings the encoder separated from the guiding rail and missed data. It may be seen that the barge reached target speed rather quickly and then traveled more or less constantly within a

moderate fluctuation of 15 percent of the target speed. The remaining three charts show current measurements at C4, C5, and C7. In these charts, independent velocities in the x, y, and z directions were denoted as "inline," "lateral," and "vertical" components, respectively. Additional runs were, for the most part, of similar quality. This report presents representative test runs that highlight the influence of the primary parameters considered.

The distance traveled by the barge over a given length of time was not constant throughout testing because not all runs were conducted at the same forward speed. Therefore, excursion distance rather than elapsed travel time provided a more consistent basis for comparing different runs. Water particle velocity measurements for the various test runs compared more consistently when expressed in terms of barge excursion distance referenced to the center of the barge. This center was aligned with the origin of the Cartesian coordinate system "O" as shown in Figure 5 at the start of a test run. The results of current velocity and forward barge speed as functions of excursion distance are displayed graphically in Figures 9 through 15. Each figure contains eight charts arranged in a consistent format. The top left chart illustrates barge speed at various positions on its course. Other parameters used are listed on this chart as well. The remaining charts present the independent components of particle velocity, taken from a group of three observation sites at a time. The 3D ADV (C7) was mounted on the barge throughout all the tests. The 2D ADVs were rotated by pairs, consisting of C1and C3, C2 and C6, and C4 and C5, so that velocity measurements could be presented in a like manner. Other captions are self-explanatory.

Actual test parameters for each run are listed in Table 1. Test runs are identified by the run number (e.g., pv11a) as shown in Table 1. Results are arranged by group to show the effects of water depth, approach speed, and approach angle. Figures 9 through 11 give a complete set of velocity measurements at all observation sites for the barge at different speeds. For this example, the water depth is 21 cm and the approach angle is zero degrees. Figures 12 and 13 present the results for approach angles of 5 and 10 degrees. Figure 14 compares the velocity measurements in three different water depths while approach speed and angle remain constant. Figure 15 illustrates the influence of approach angle at constant water depth and approach speed.

The floating ping-pong balls and the submersed neutrally buoyant beads demonstrated the gross flow patterns induced by the berthing barge. Floating balls deposited 1 meter or less behind the barge at the start of the test caught up and stuck to the barge as it moved forward, clinging to it for the remainder of the journey. Balls deposited in excess of 2 meters also moved forward in the direction of the barge, but continued to fall farther and farther behind the barge as it traveled down its course. Floats placed initially near midship moved in nearly straight lines during a test run, while those deposited outside the middle one-third of the barge length moved initially in straight lines, but gradually drifted away from midship as the barge stopped. These gross tendencies were most pronounced at the higher approach speeds in shallow water when floats generally spread over the entire excursion distance and continued to drift into the quay wall for some time after the barge had stopped. A conclusion drawn from these observations is that a berthing barge, even when traveling at a low speed, does draw a substantial amount of trailing water behind it.

In "deep water" trials (35-cm water depth), the neutrally buoyant beads submersed at the first location were swept almost indiscernibly back from the quay wall as the barge passed overhead. In shallow water trials (21-cm water depth), the first location beads were diverted obliquely from the direction of barge motion roughly 45 to 60 degrees. The beads at the second

location (0.5 meter away from the quay wall) were for the most part displaced parallel to the quay wall as the barge approached, remaining trapped underneath after the barge stopped. The beads deposited at the third location (inside the north end of the barge) expressed a pronounced, counterclockwise recirculation in the shallow water runs. Similar but weaker patterns of recirculation were also observed in the deep water cases. In all test runs, the submersed beads were lifted slightly from the bottom floor of the basin.

Results of the numerical simulation for test run pv21b are presented in Figures 16 through 20 to demonstrate the general features and capabilities of the simulation model (refer to Refs 3 and 4 for additional details). For this example run, the barge traveled at 10 cm/sec (length parallel to the quay wall) in water 21 cm deep. The barge motion was approximated by a constant forward speed and ramp start/stop acceleration that modeled test conditions, as shown in Figure 8. Figure 16 shows the computational domain and numerical grids at the beginning and the end of the simulations. The 31 X 21 X 41 boundary-fitted barge grid is allowed to move with respect to the 31 X 251 X 21 basin grid at barge speed. The simulations were conducted for 540 time steps with a total duration of 72.5 seconds. The barge, initially accelerated from 0 to 10 cm/sec in 4.6 seconds, maintained that speed until decelerating at the end of 64.4 seconds travel time to a complete stop in 2.3 seconds. Figures 17 and 18 show the computed velocity contours in terms of lateral (y-axis) and inline (x-axis) components. The results clearly indicate the presence of large recirculating patterns on the free surface. A strong, underkeel flow acceleration is also observed in the center plane of symmetry.

Figures 19a through 19d show the progressive change in the fluid velocity vector field predicted by the simulation model. During the acceleration period (ending at 4.65 seconds) as shown in Figure 19a, a significant portion of the fluid directly in front of the barge was pushed back under the keel while fluid immediately under the barge keel was drawn forward due to viscosity effects. As the vessel attained constant speed and continued forward (Figure 19b), the backflow decreased, indicating that more of the displaced fluid before the barge was being directed around the ends of the barge. As the barge approached its stopping location with the quay wall distance decreasing (Figure 19c), the amount of trapped fluid pushed back under the keel increased substantially, and a visible recirculation behind the barge developed. After the barge came to a sudden stop at 65.1 seconds, the simulation indicated that the backflow under the keel diminished gradually. However, the trailing current continued to move forward, pushing its way through the underkeel clearance, as shown in Figure 19d. Figure 20 compares the velocity history predicted by the simulation to that observed at the model basin. The simulation model appears to capture most of the critical features of the transient flow observed in the model basin.

REMARKS AND FINDINGS

1. The simple model setup was able to reproduce most of the critical features of the transient flow regime induced by a berthing barge. The ADV current meters were effective in capturing rapidly changing water movement. The potentiometer provided a record of overall barge excursion. A number of problems attributed to unsteady travel of the towing carriage were observed during the tests. As a result, the flow fields generated were somewhat more complicated than desired. Nevertheless, the general pattern of flow

observed and recorded was sufficiently clear to guide the development of a numerical simulation. Strong electrical noises were also picked up while recording raw data. This high frequency noise was successfully screened from current measurements by a low-pass filter. The quality of the measurements is discussed later.

2. The towing carriage could not move the barge forward at a constant approach speed as desired. Forward travel of the carriage was also somewhat jerky due to surface irregularities on the guiding rails. As a result, the actual approach speed of the barge varied typically within about 15 percent of the target speed. The result of unsteady forward travel and erratic oscillation was the introduction of unwanted fluctuations within the developed current. However, when viewed on a gross scale, the general pattern of flow appeared stable.

3. In some of the shallow water runs, the barge appeared to strike a small protrusion at the bottom of the tank, creating brief but significant surge and roll. This situation occurred most frequently when the barge traveled at the highest test speed of 20 cm/sec, as shown in the top left chart of Figure 9. The resulting impulse motion (recorded during run pv31a) induced sudden changes in the local current field in the inline (Figure 9b) and vertical (Figure 9d) directions, as recorded by the barge- mounted current meter, C7. Other current meters were much less affected. The motion also induced a noticeable wave train that was trapped between the quay and barge for the remainder of the test run. Wave activity is reflected in the strong oscillation of C7 measurements.

4. The barge appeared to be too heavy for positive handling by the towing carriage. As the barge decelerated to a quick stop before the quay wall, its stopping produced a pronounced vertical vibration, inducing a dominating current activity that is not a normal characteristic of actual berthing operations. Because this vibration was not monitored during the actual test, it was difficult to interpret the current activity after the barge stopped.

5. A particular test could be repeated reasonably well even though it was not possible to duplicate the precise history of carriage movement from run to run. Figures 21 through 23 present the component velocity measurements recorded at station C7 for the "a" and "b" runs in tests pv11, pv31, and pv61, respectively. The top left chart in each figure compares the movement history of the carriage. The remaining three charts compare the corresponding component velocities in three spatial directions measured at C7. In spite of the erratic nature of carriage travel, the measurements of component velocities between runs of identical test parameters correlated well.

6. In all test runs the berthing barge drew a significant volume of trailing water behind it. The movement of trailing water persisted even after the barge stopped. The barge also pushed a substantial volume of water in front; however, the distance of influence seemed to be shorter than that of trailing water, as indicated by the moving ping-pong ball floats.

7. The inline velocities associated with reverse flow around the ends of the berthing barge were comparable in magnitude to the approach speed, as indicated by measurements recorded at C7. The C7 gauge (mounted on the bare barge) measured an inline water particle velocity of approximately 20 cm/sec relative to the direction opposite to barge motion, as shown in Figure 8 (test pv21b). This water particle velocity is actually the sum of the carriage speed forward and the underkeel flow backward. In this particular run, the barge was traveling at 10 cm/sec forward, thus the velocity of the fluid was approximately equal to that of the barge but in the opposite direction .

8. Significant towing force is required to maintain the barge at a constant speed. The large amount of power required to draw the barge forward at a constant speed confirms the existence of a significant drag force. Form drag represents the majority of the fluid-induced resistance. This force cannot be represented simply by added mass as the barge was essentially moving at constant speed. A similar effect is experienced when the trailing body of water pushes the barge into the quay wall after the barge comes to a sudden stop. This force is not accounted for in the current design practice.

9. As the distance between the barge and the quay wall closed, there was increasing alignment between the direction of flow of water pushed in front of and beneath the barge and the quay wall. Symmetry prevailed in lateral directions so that the flows at gauges C2 and C6, mirror images of one another across the centerline of the barge, were directed toward the south and north ends of the basin, respectively. Figure 24 illustrates this feature by comparing the velocity components observed at C2 and C6 for both the shallow water (left charts) and deep water (right charts) conditions. There is good correlation between the two records for each of the charts. In this figure, the sign of the lateral velocity component at C2 has been reversed for ease of comparison. This trend toward symmetry is clearly illustrated in Figure 25, which presents measured flow velocity in vector format in terms of magnitude (charts b, e, and g) and direction (charts c, f, and h). Figure 25d illustrates the layout of current meters. It may be seen that current measurements at C2 and C6 are comparable in magnitude (Figure 25b) and similar in angular departure from the barge heading (Figure 25c). This condition is shown pictorially in Figures 26, 27, and 28, which indicate flow direction and magnitude at barge excursion distances of 300, 400, and 500 cm from its starting position, respectively.

10. Because successive test runs (in which the pair of 2D ADV meters was relocated) were repeated with sufficient consistency, it is instructive to compare current measurements at all six locations of velocity meters C1 through C6. The symmetry of C2 and C6 was established in the previous paragraph. Figures 25 to 28 are instructive in describing the condition at C1, C3, C4, and C5 also. For purposes of discussion, it is useful to pair C4 with C3 because these two locations are equally distant from and closest to the quay wall. As the barge approached the quay wall, the flows recorded at C4 and C3 increased together while maintaining the same direction, pointing away from the barge. The angle of departure increased toward 90 degrees as the barge approached the quay wall and as water was "squeezed" to the sides. Likewise, C5 and C1 are paired because they were

equally distant from the quay wall (but farther away than C3 and C4). At the barge excursion of 300 cm, the magnitude and direction of flow past C1 and C5 were about the same. As the barge advanced to 400 cm, the magnitude increased (about the same) at both locations, and the directions changed rapidly. This trend was most pronounced as the barge passed directly over C5 (at an excursion distance of about 440 cm) and the flow direction swung suddenly from -60 to -120 degrees. The velocity at C5 (which was beneath the barge) increased suddenly and maintained the higher magnitude while the velocity at C1 (which was at mid-water depth outboard of the barge) decreased gradually. As the barge passed over C5 on to the 500-cm excursion point, the dramatic flow reversal continued as water was pushed back under the keel. The angle of departure changed suddenly from about 60 degrees to a larger angle pointing opposite to barge movement. As soon as the forward travel of the barge was halted (just short of the quay wall at an excursion distance of about 600 cm), all current meters recorded a rapid return of flow to the forward direction (i.e., 0 degrees as shown in Figures 25c, 25f, and 25h) because the mass of water that had been trailing the barge continued to push forward.

11. As the barge passed over gauge C5, there was a pronounced flow reversal observed in the inline particle velocity. During barge approach, the gauge registered increasing positive particle velocity (the barge was pushing water forward), but a sudden reversal in water particle velocity occurred as the barge passed over the gauge and the gauge recorded the strong return flow under the barge. This may be seen in the third chart of Figure 8.

12. As the barge began its approach toward the quay wall, it dragged a significant volume of water behind it. This tendency was observed at the water surface by the forward motion of ping-pong balls that were deposited behind the barge. The inline particle motion measured by gauge C7 on the barge exhibited strong negative underkeel flow prior to stopping the barge at the quay wall (Figure 21). Flow changed rapidly to the positive direction after the barge came to a stop at the final excursion distance of about 600 cm. This positive direction flow which acted along the back surface of the barge accounted for the so-called "added mass" effect which is a well known phenomenon in ship berthing practice.

13. The vertical component of the water particle velocity measured by gauge C7 exhibits an analogous pattern (Figure 21d) to that of the inline component. Prior to wall contact, there is flow in the downward direction as the water flow behind the barge pushes into and under the barge to create a flow reversal in the upward direction at the forward edge of the barge.

14. The foregoing pattern is also observed for the lateral component of water particle motion, as measured by gauge C7 mounted on the barge. Prior to stopping, the lateral flow is from the center of the barge to either ends of the barge. After barge motion has ceased, the captured water behind the barge flows around both ends of the barge as indicated by the abrupt change in the lateral flow direction.

CONCLUDING REMARKS

Sensitive, state-of-the-art acoustic-type doppler velocity current meters were used to accurately measure the motion of water particles around the model of a berthing barge. Evidence of entrained flow, underkeel flow, and reversed flow resulting from abruptly arresting the forward motion of the barge was observed.

The large volume of trailing water was found to contribute significantly to the resulting berthing energy, especially in runs where water depth was small in comparison to ship draft. Within the range of parameters validated in these particular tests, the influence of the approach angle was found to hold less significance, as indicated by the minor changes in the water flow induced by the barge approaching at different magnitudes of angle.

Excellent comparisons of measured and predicted water currents around a berthing barge were noted for the deepest water series of tests. Comparisons for the two shallower water tests were not as noteworthy, and this discrepancy may be attributed to the somewhat erratic forward motion of the barge.

REFERENCES

1. Naval Facilities Engineering Service Center. Technical Memorandum TM-2094-SHR: Ship berthing forces - Initiation decision Report, by D. A. Davis and E. T. Huang. Port Hueneme, CA, Sep 1994.

2. Naval Facilities Engineering Command. Military Handbook 1025/1: Piers and wharfs. Alexandria, VA, 30 October 1987.

3. M. Chen, H. Chen, and D. Davis. "Numerical simulation of transient flows induced by a berthing ship," in Proceedings: International Society of Offshore and Polar Engineers, Los Angeles, CA, 1996.

4. H.C. Chen, T. Liu, M. Chen, E.T. Huang, and D.A. Davis. "Validation of Chimera RANS/free-surface method for time-domain simulation of a berthing barge," 12th ASCE Engineering Mechanics Conference, La Jolla, CA, May 17-20, 1998.

Table 1. Text Matrix

Run Number	Current Meter Locations			Water Depth	Approach Angle	Approach Speed
	0 (2D)	1 (3D)	2 (2D)	(cm)	(degrees)	(cm/sec)
pv11a	c2	c7	c6	21	0	5
pv21a	c2	c7	c6	21	0	10
pv31a	c2	c7	c6	21	0	20
pv11b	c4	c7	c5	21	0	5
pv21b	c4	c7	c5	21	0	10
pv31b	c4	c7	c5	21	0	20
pv11c	c1	c7	c3	21	0	5
pv21c	c1	c7	c3	21	0	10
pv31c	c1	c7	c3	21	0	20
pv41a	c2	c7	c6	26.7	0	5
pv51a	c2	c7	c6	26.7	0	10
pv61a	c2	c7	c6	26.7	0	20
pv41b	c4	c7	c5	26.7	0	5
pv51b	c4	c7	c5	26.7	0	10
pv61b	c4	c7	c5	26.7	0	20
pv41c	c1	c7	c3	26.7	0	5
pv51c	c1	c7	c3	26.7	0	10
pv61c	c1	c7	c3	26.7	0	20
pv71a	c2	c7	c6	35	0	5
pv81a	c2	c7	c6	35	0	10
pv91a	c2	c7	c6	35	0	20
pv71b	c4	c7	c5	35	0	5
pv81b	c4	c7	c5	35	0	10
pv91b	c4	c7	c5	35	0	20
pv71c	c1	c7	c3	35	0	5
pv81c	c1	c7	c3	35	0	10
pv91c	c1	c7	c3	35	0	20
pv12a	c2	c7	c6	21	5	5
pv22a	c2	c7	c6	21	5	10
pv32a	c2	c7	c6	21	5	20
pv12b	c4	c7	c5	21	5	5
pv22b	c4	c7	c5	21	5	10
pv32b	c4	c7	c5	21	5	20
pv12c	c1	c7	c3	21	5	5
pv22c	c1	c7	c3	21	5	10
pv32c	c1	c7	c3	21	5	20
pv13a	c2	c7	c6	21	10	5
pv23a	c2	c7	c6	21	10	10
pv33a	c2	c7	c6	21	10	20
pv13b	c4	c7	c5	21	10	5
pv23b	c4	c7	c5	21	10	10
pv33b	c4	c7	c5	21	10	20
pv13c	c1	c7	c3	21	10	5
pv23c	c1	c7	c3	21	10	10
pv33c	c1	c7	c3	21	10	20

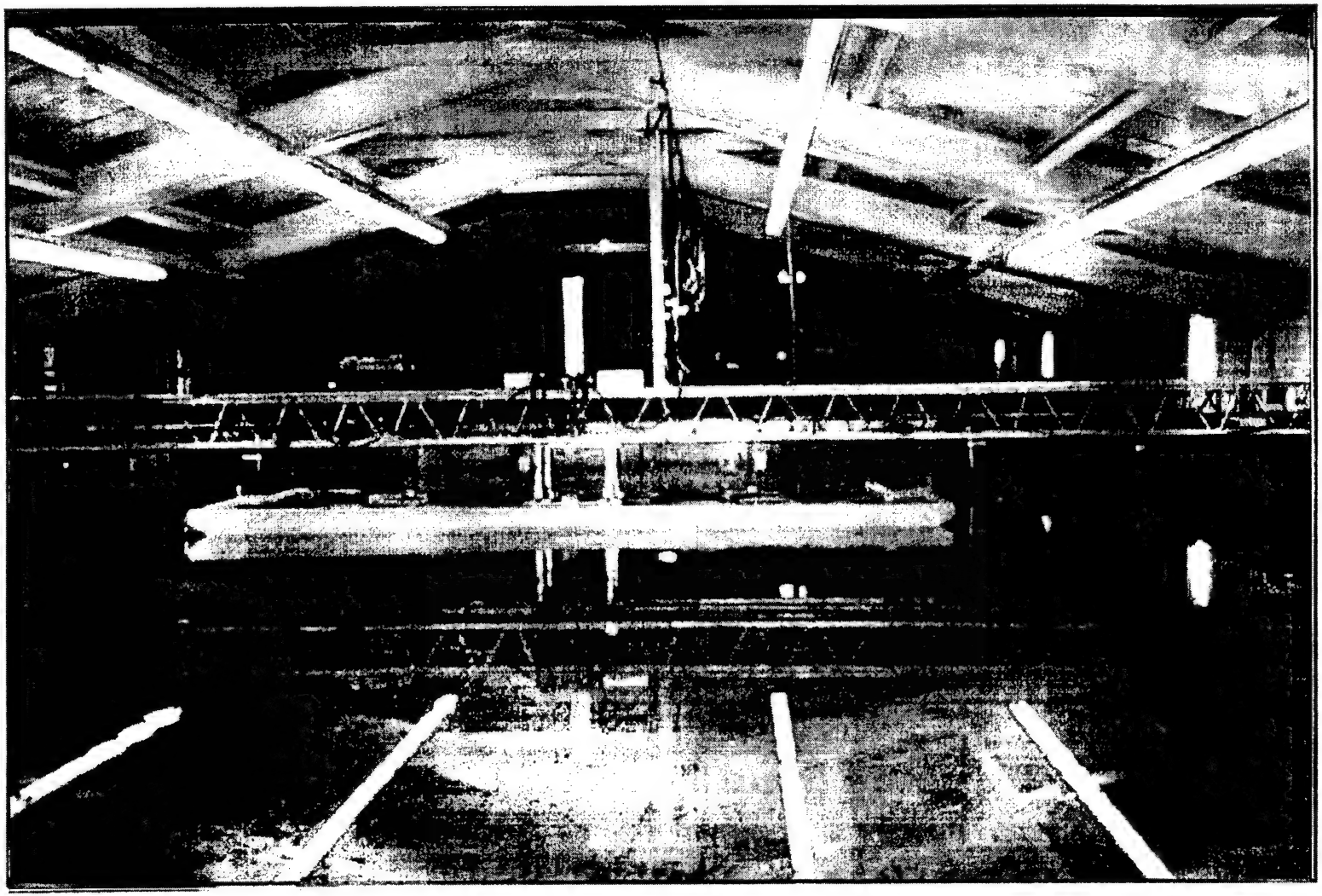

Figure 1. Test facility.

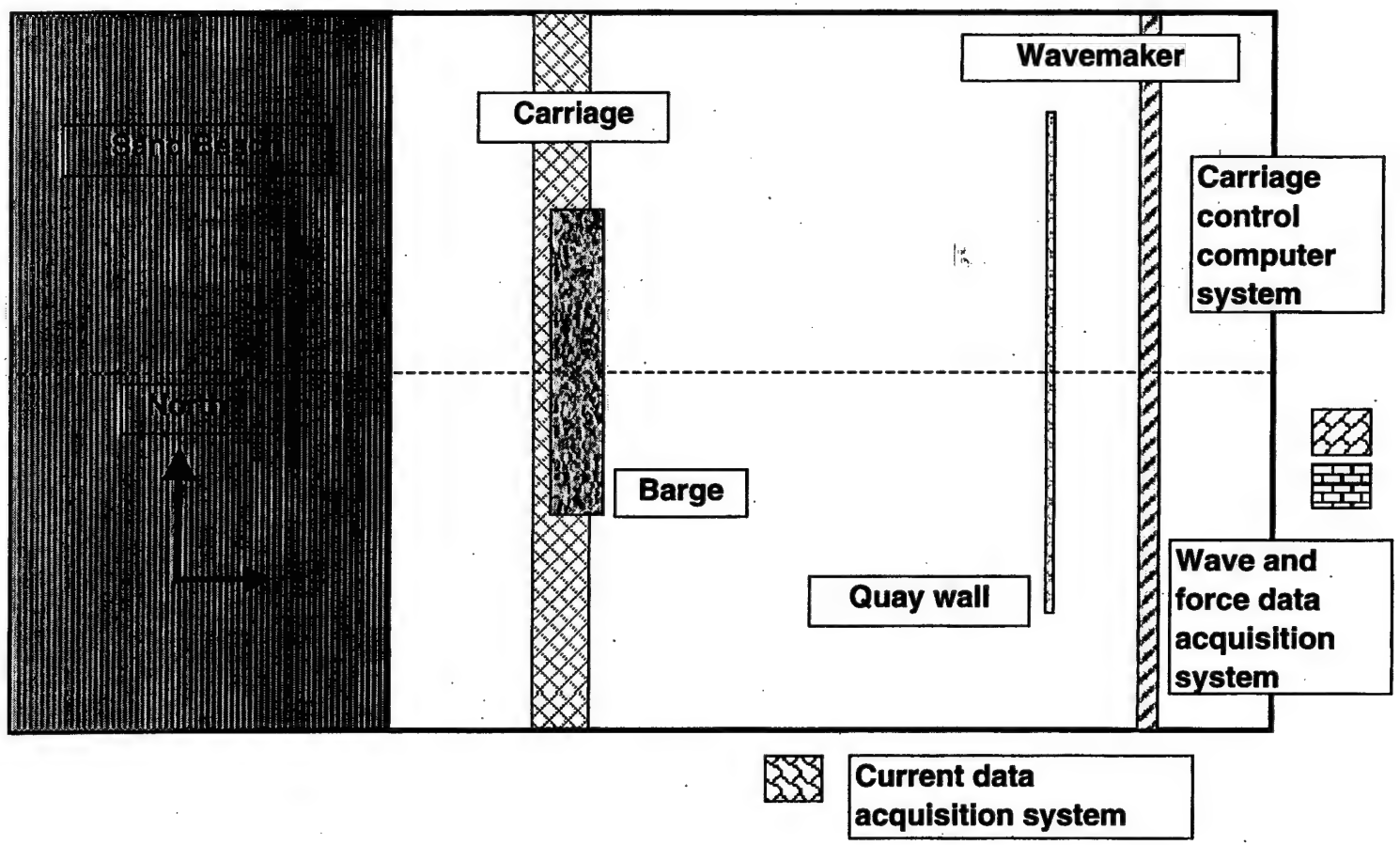

Figure 2. Test layouts.

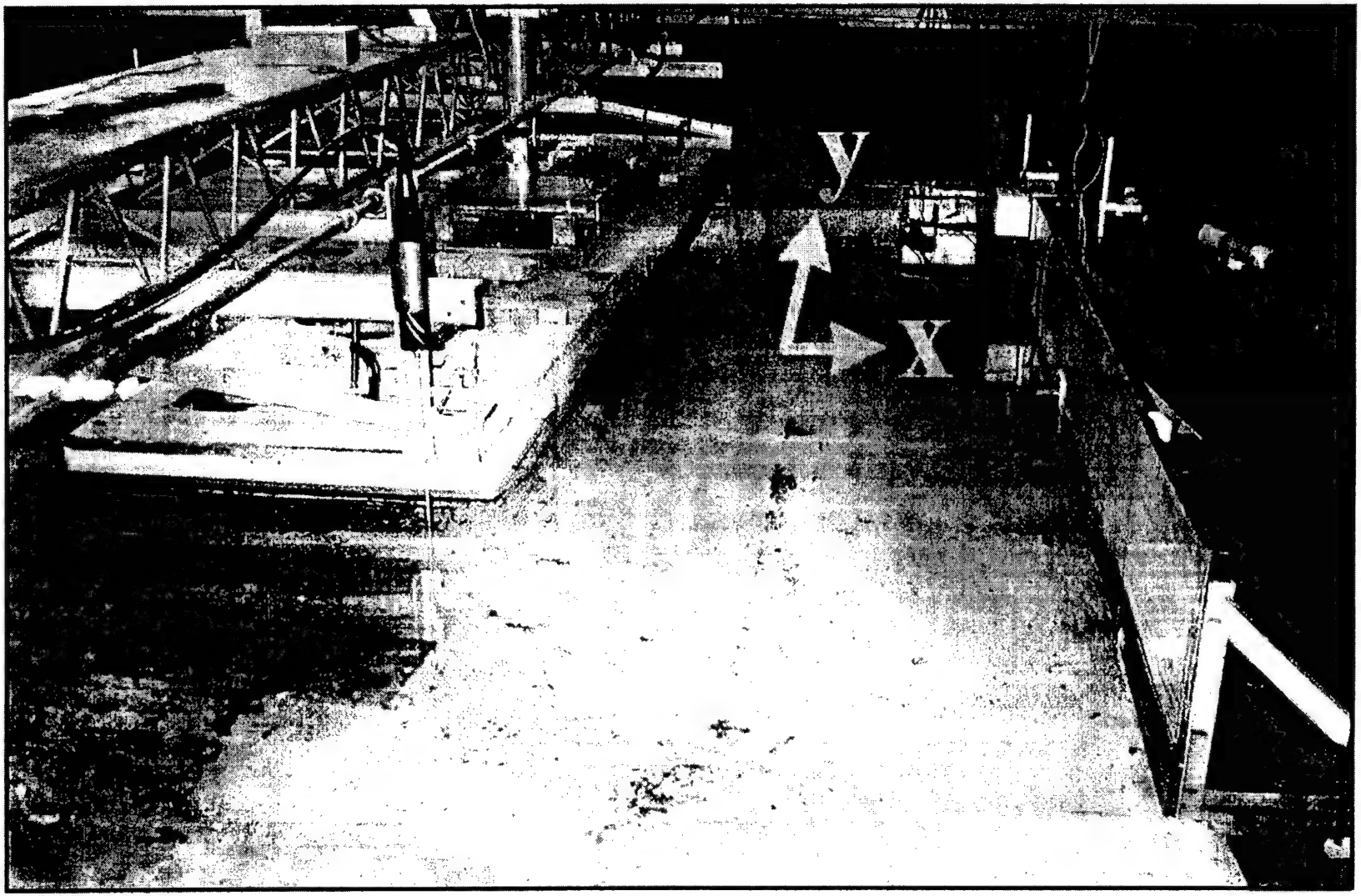

Figure 3. Barge model and instrumentation setup.

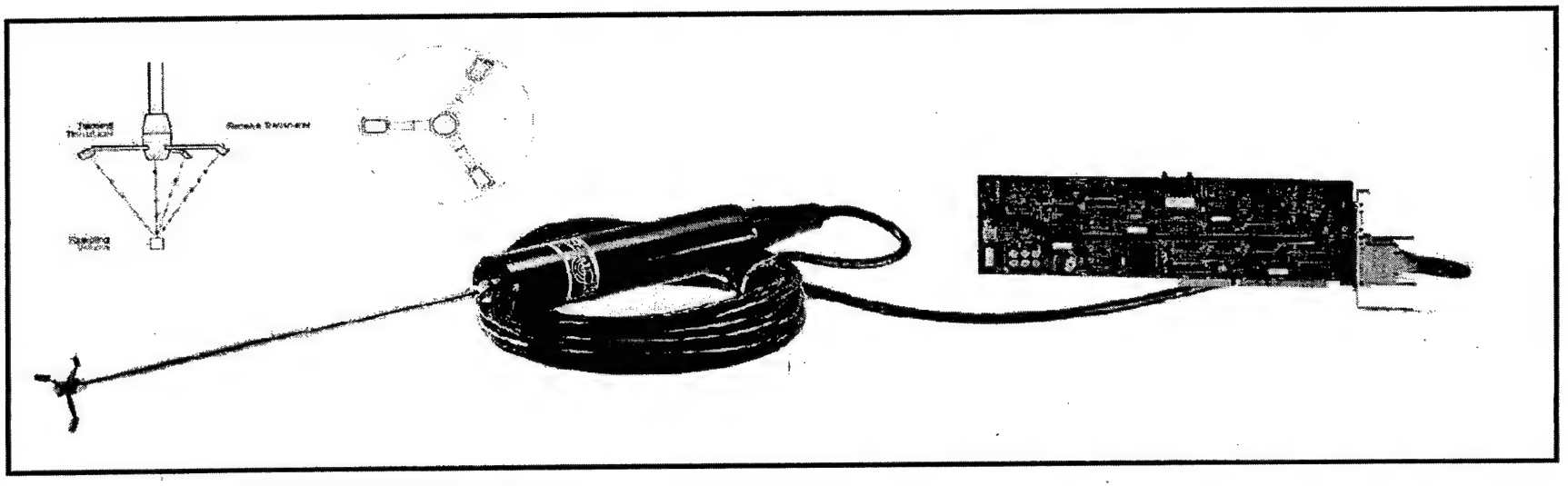

Figure 4. Acoustic Doppler Velocity (ADV) meter.

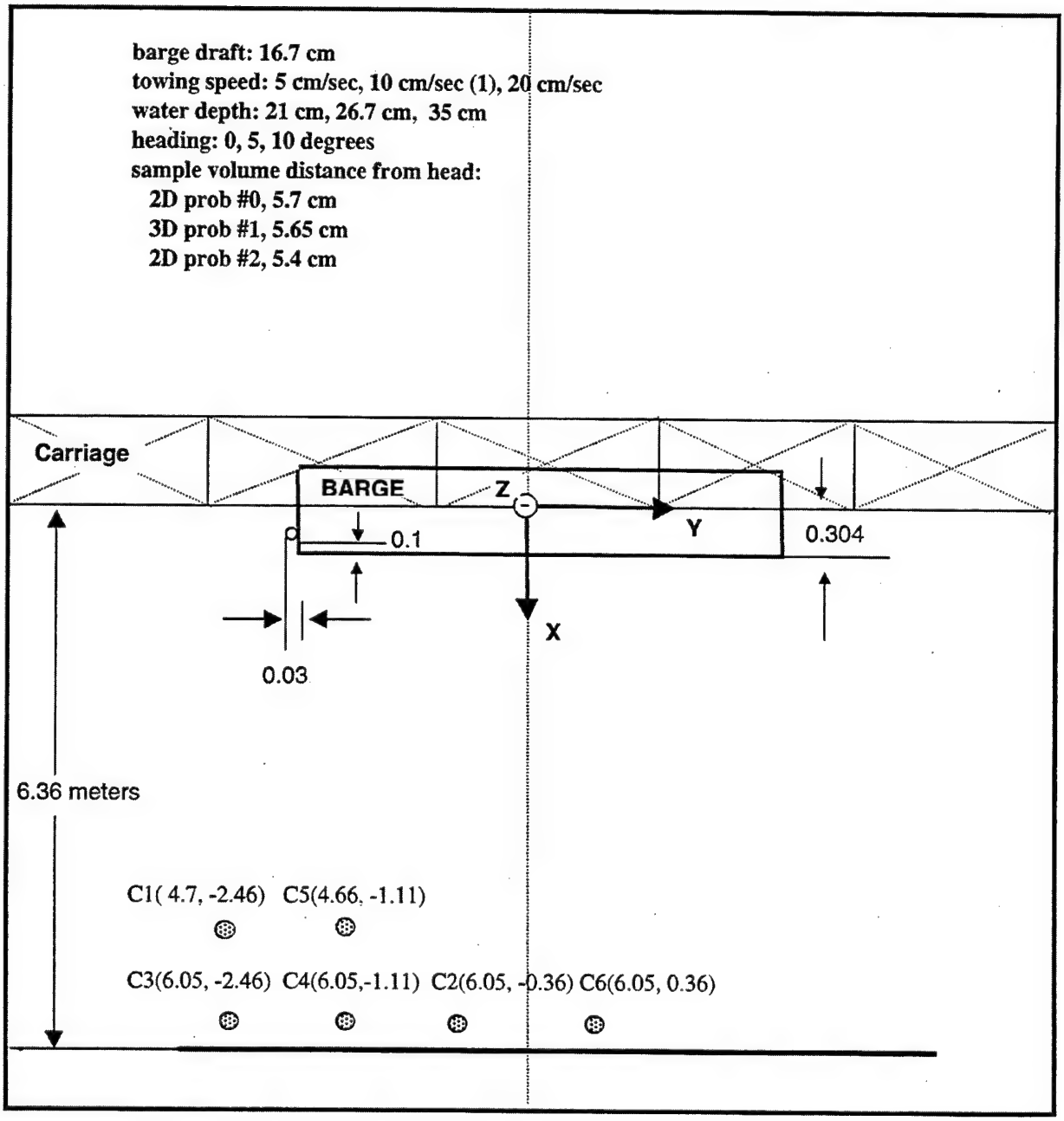

Figure 5. Experimental setup.

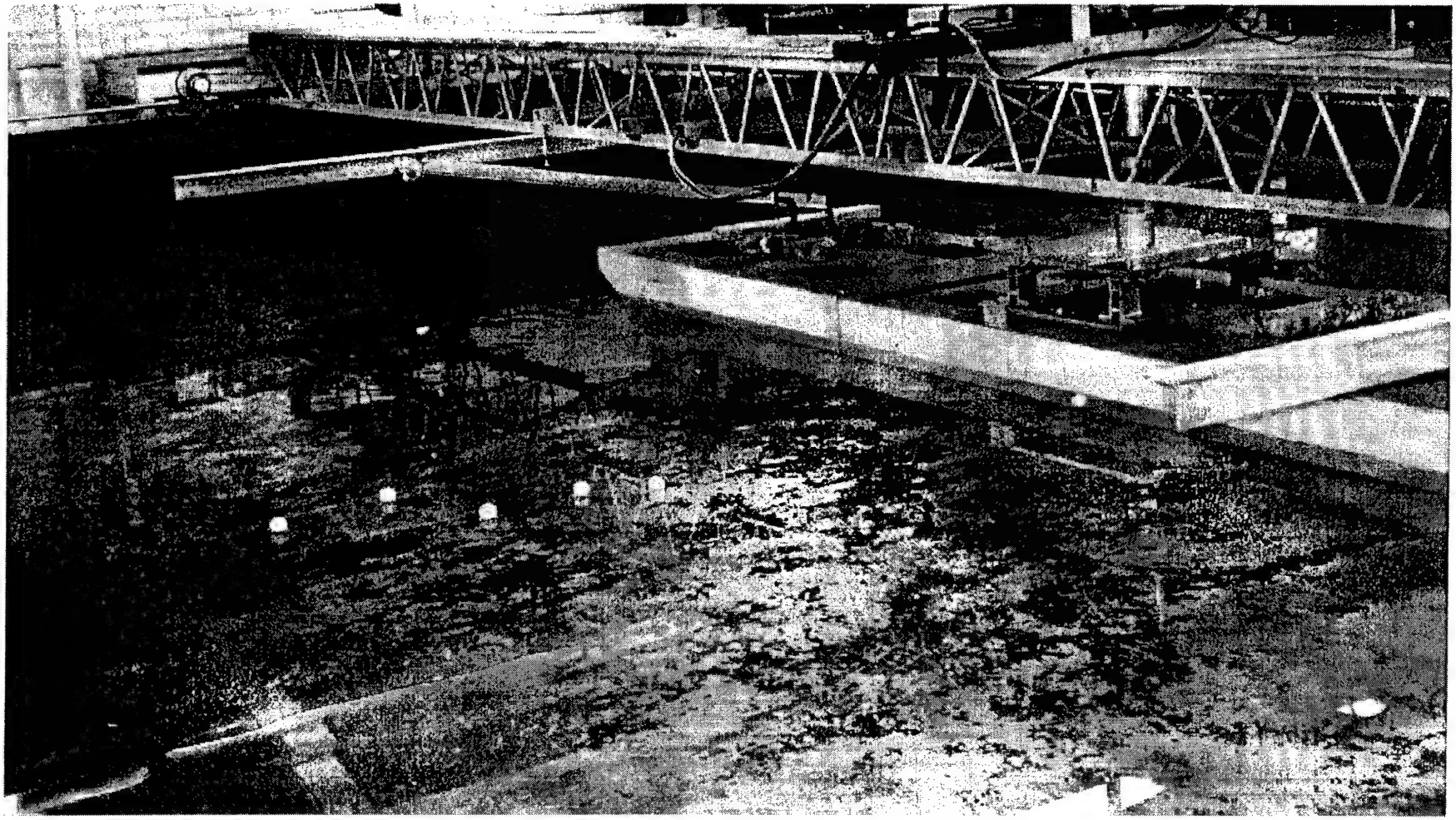

Figure 6. Surface flow pattern.

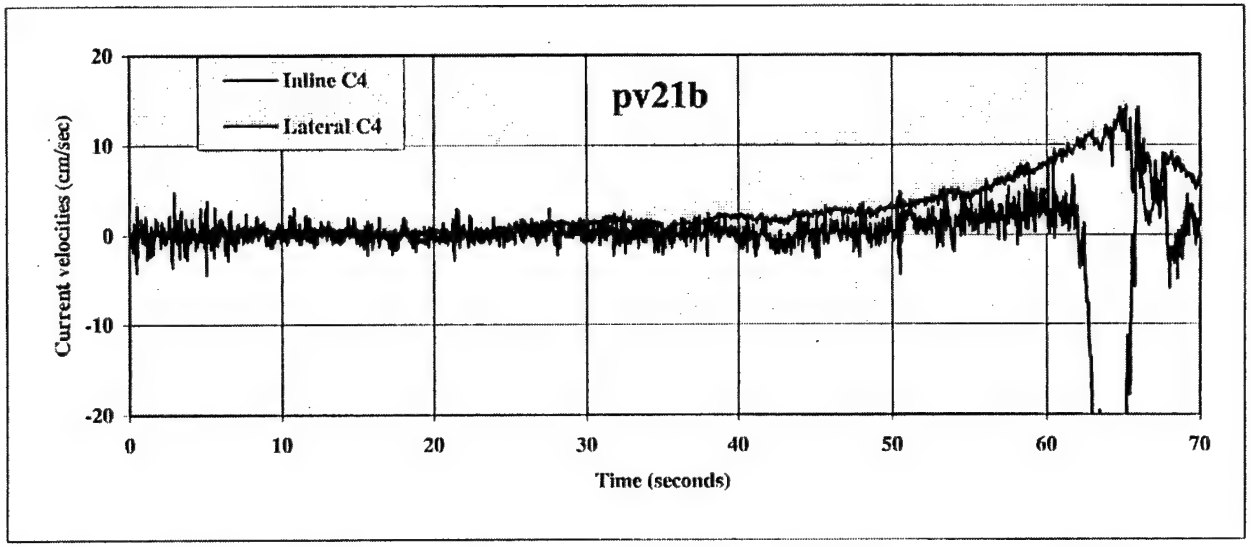

Figure 7. Sample raw data of current meter measurements.

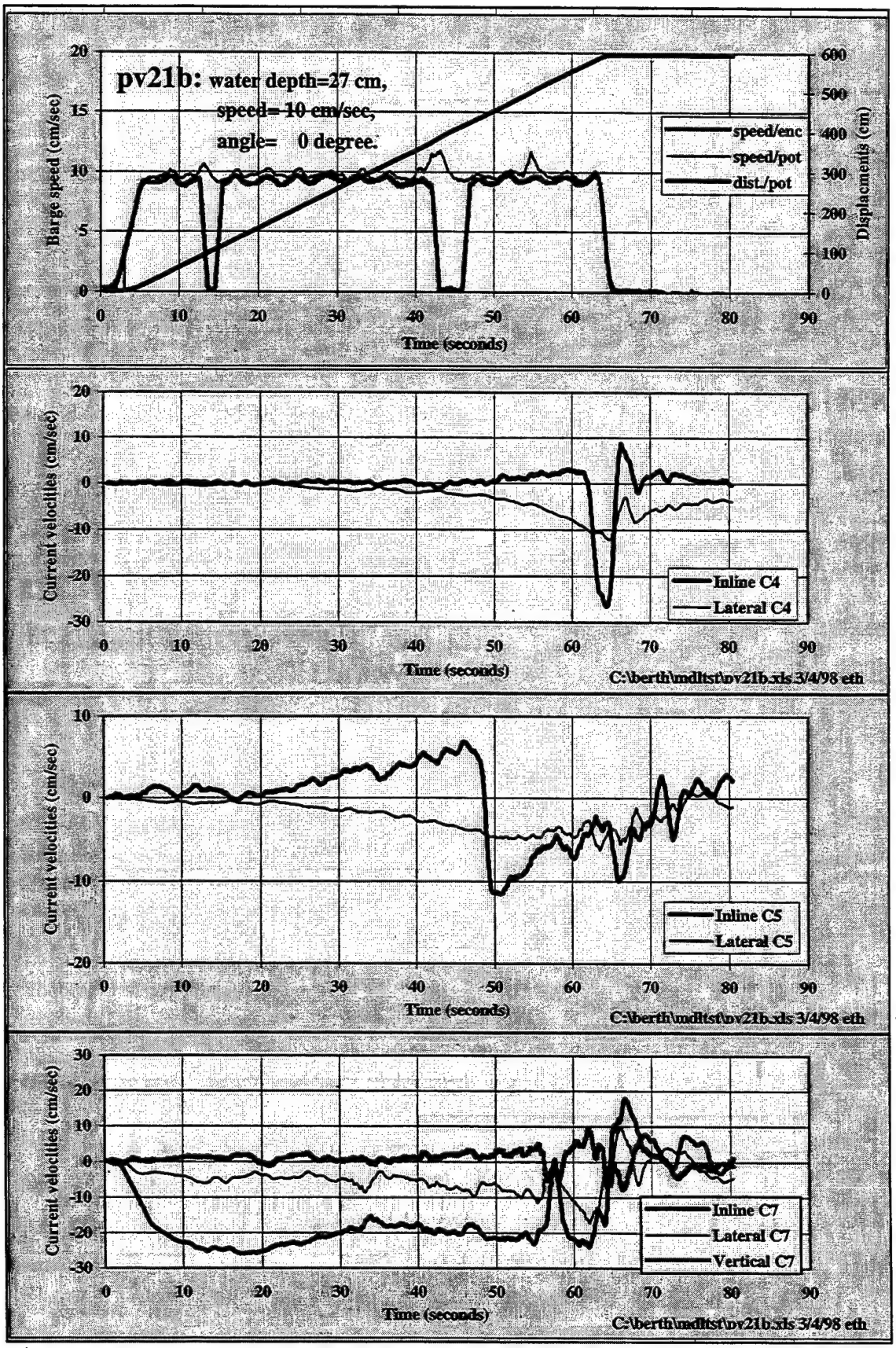

Figure 8. Examples of filtered data of barge motion and current measurements.

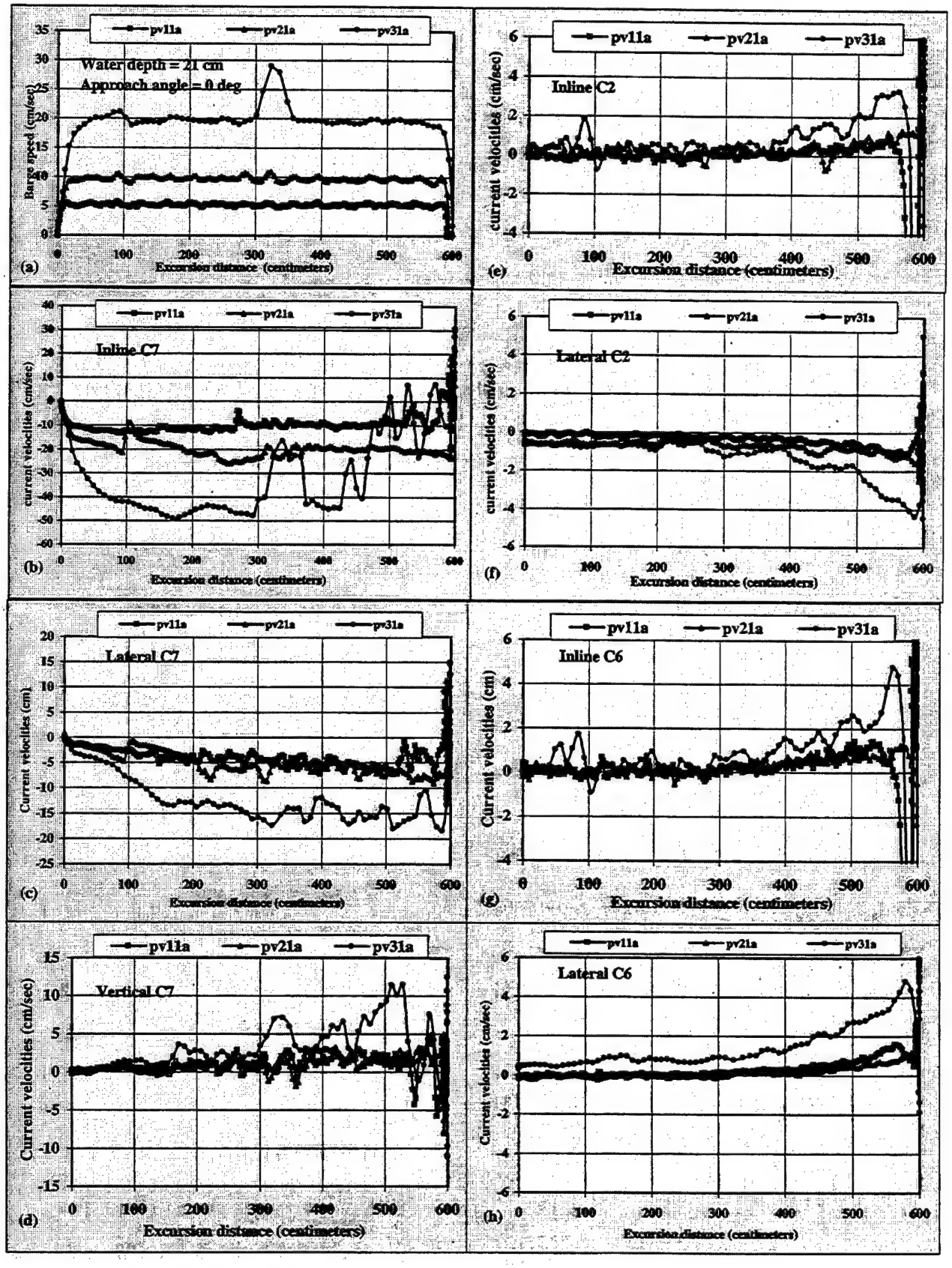

Figure 9. Current measurements at C2, C6, and C7 for water depth = 21 cm and approach angle = 0 degree.

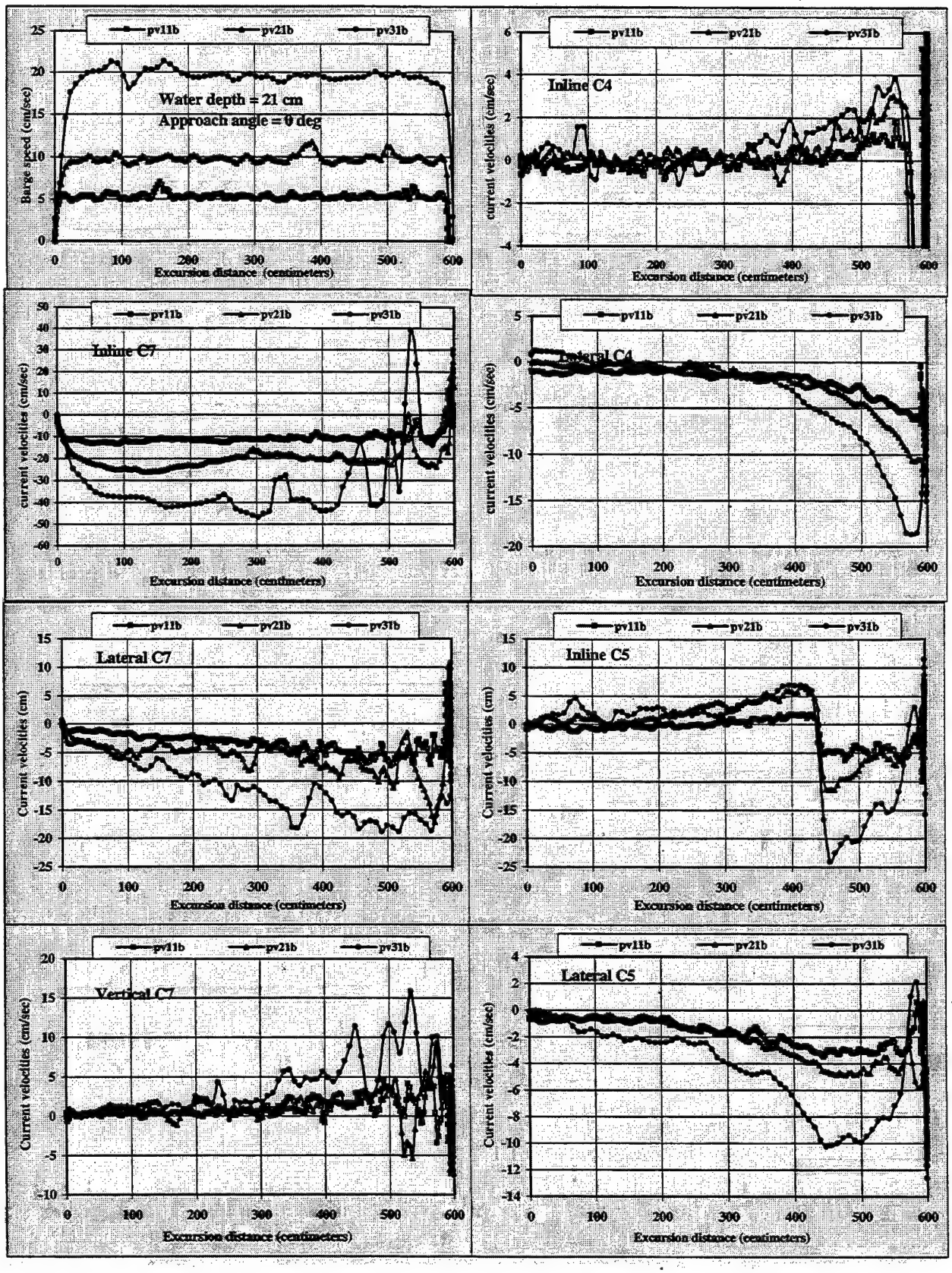

Figure 10. Current measurements at C4, C5, and C7
for water depth = 21 cm and approach angle = 0 degree.

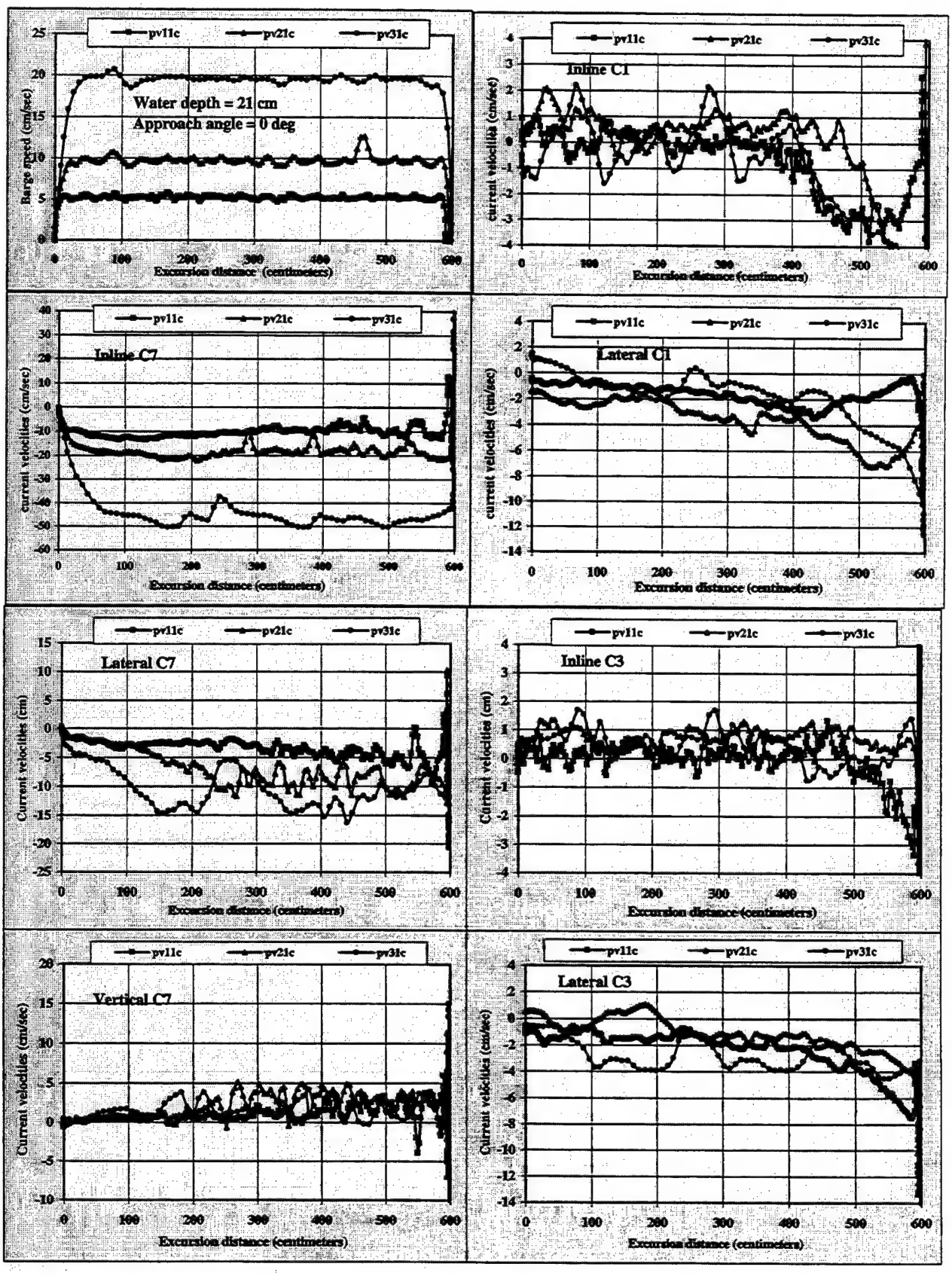

Figure11. Current measurement at C1, C3, and C7
for water depth = 21 cm and approach angle = 0 degree.

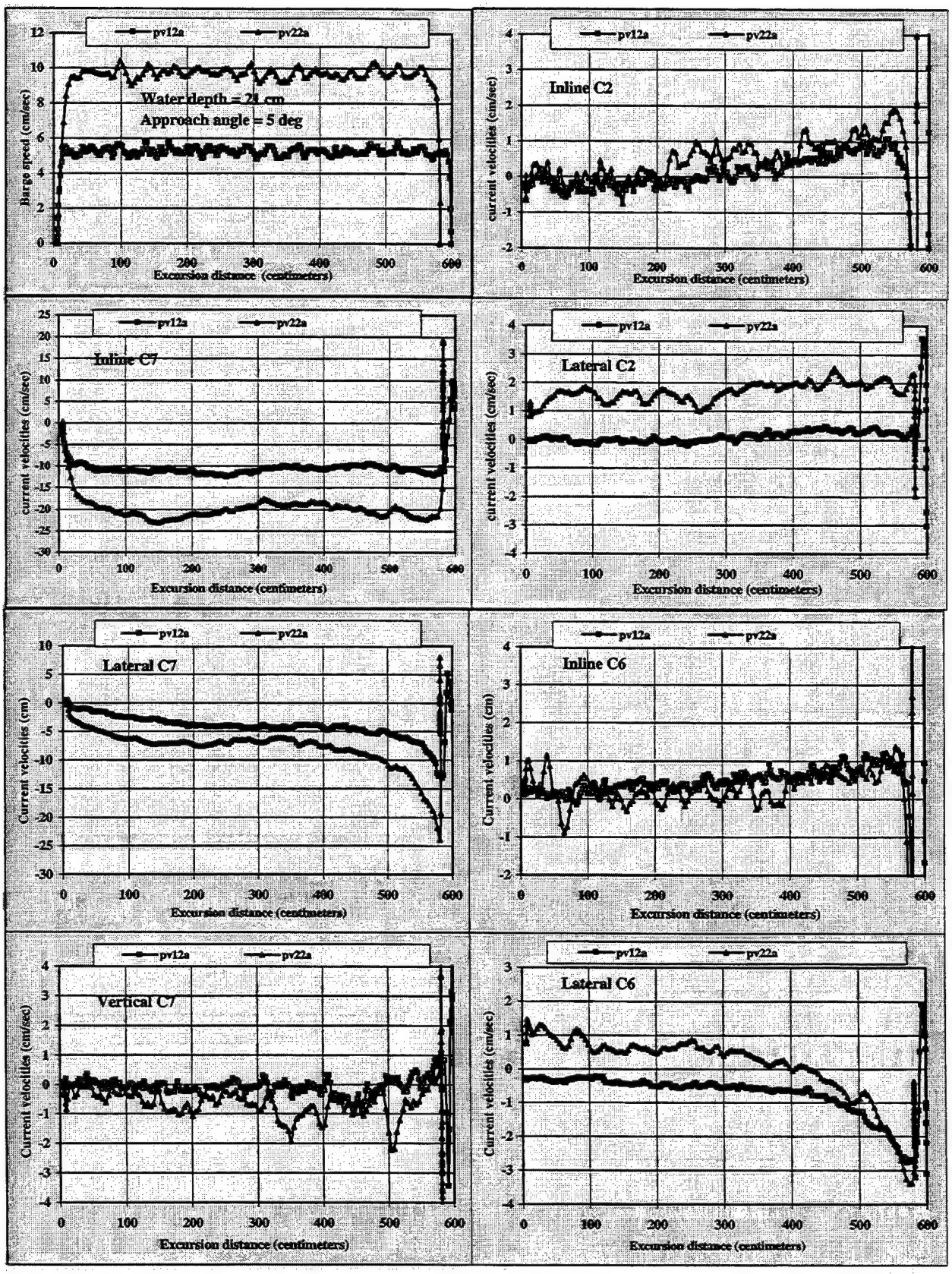

Figure 12. Current measurement at C2, C6, and C7
for water depth = 21 cm and approach angle = 5 degrees.

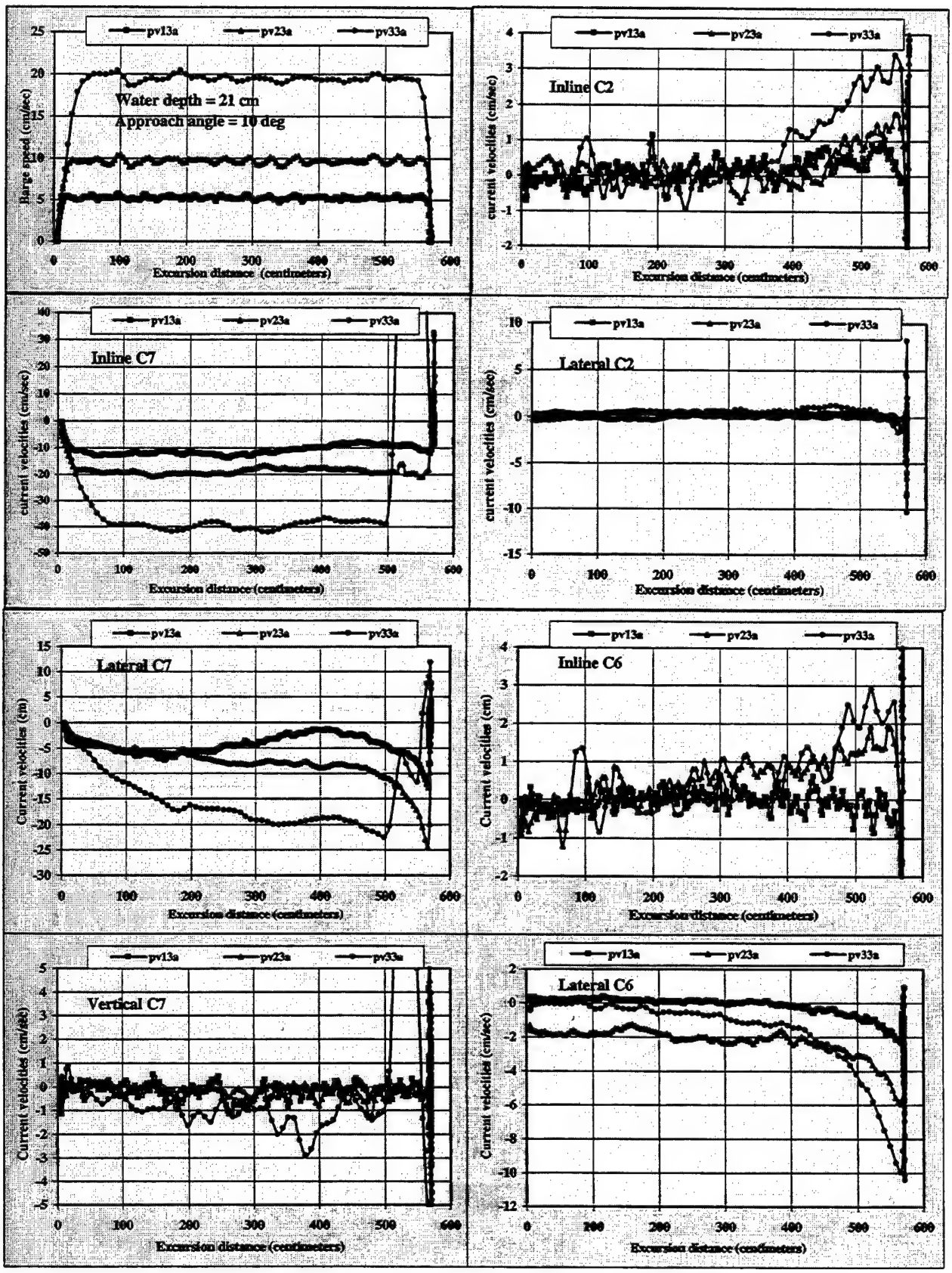

Figure 13. Current measurements at C2, C6, and C7
for water depth = 21 cm and approach angle = 10 degrees.

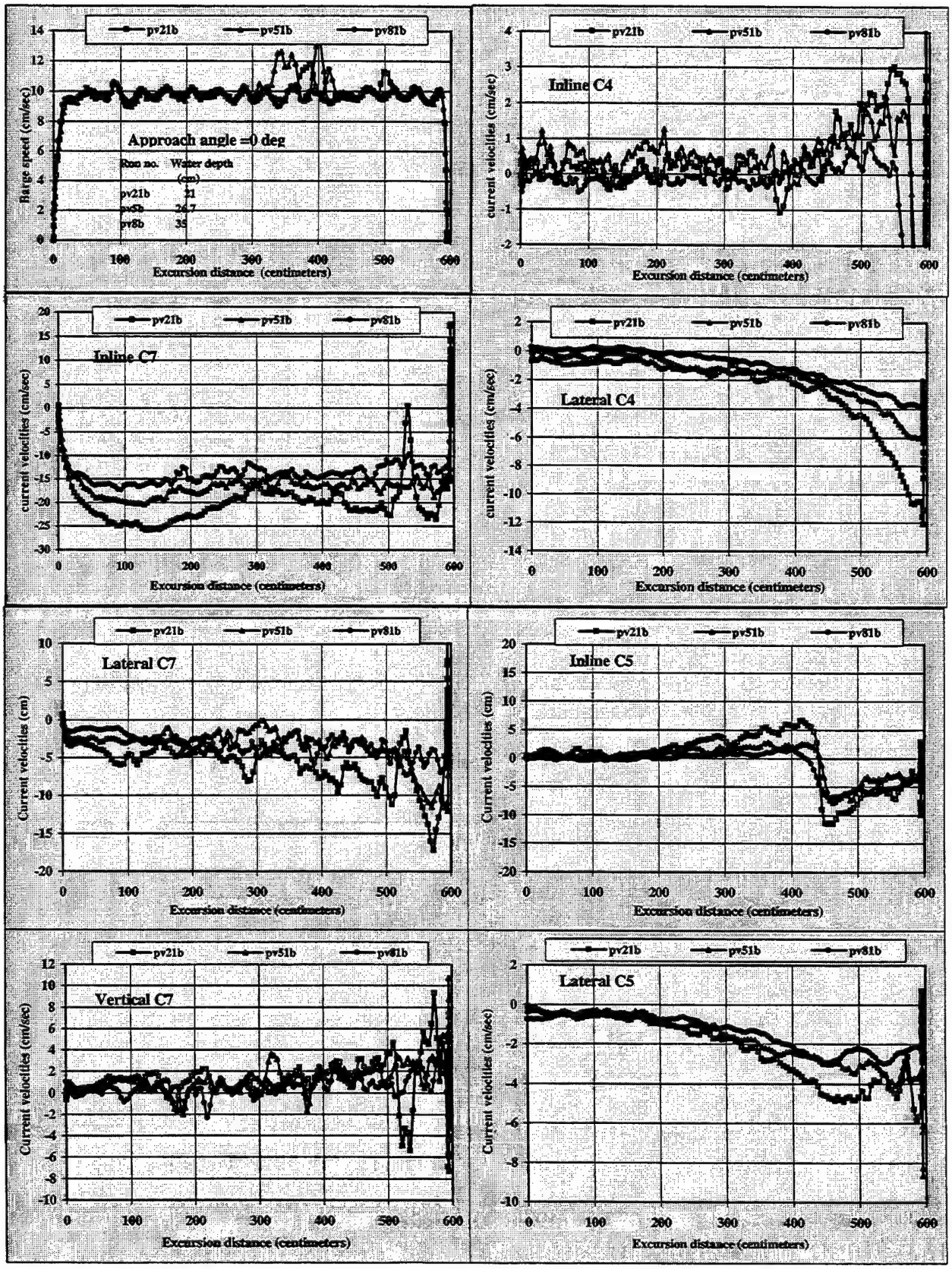

Figure 14. Influence of water depth on currents.

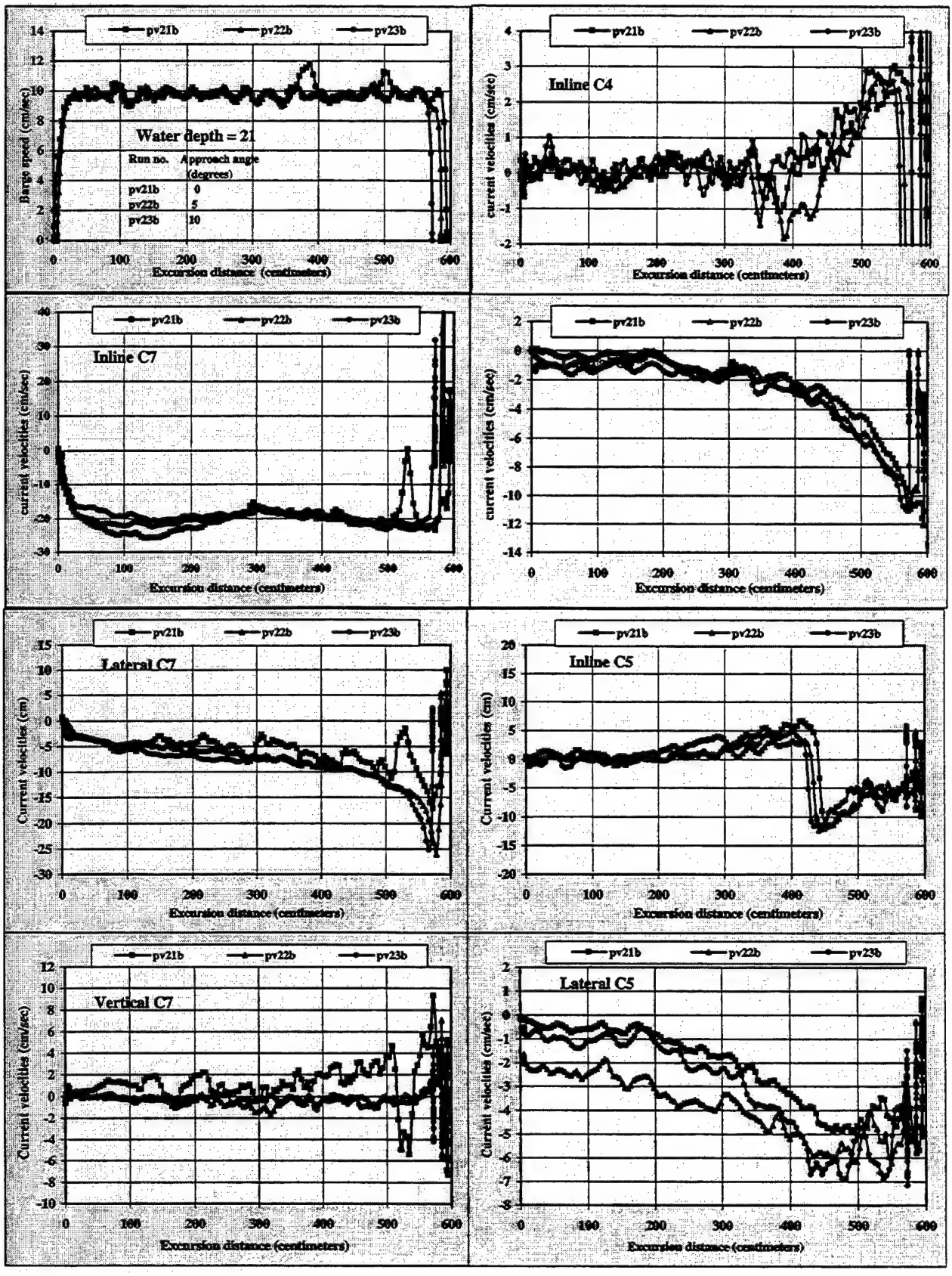

Figure 15. Influence of approach angle on currents.

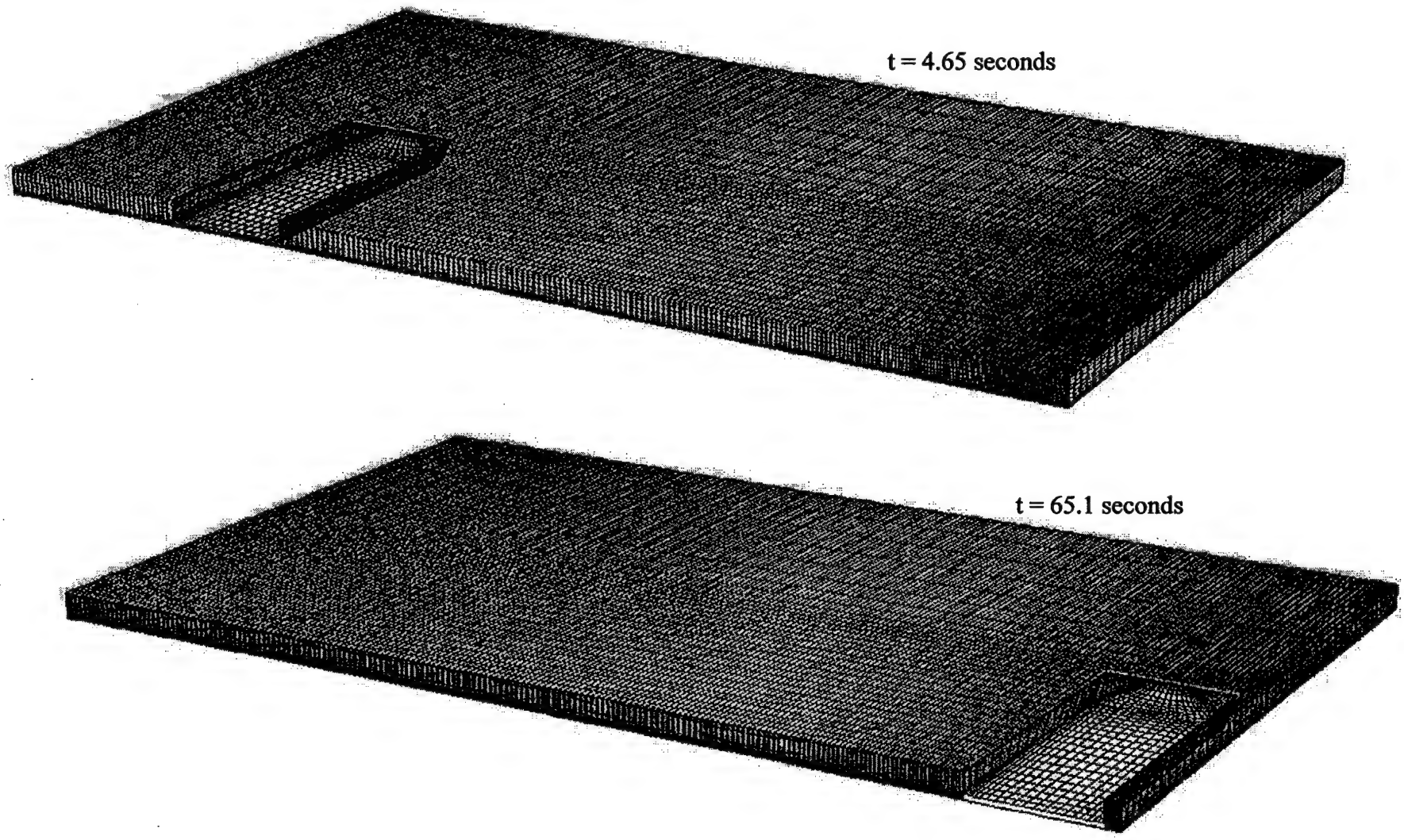

Figure 16. Solution domain and numerical grids.

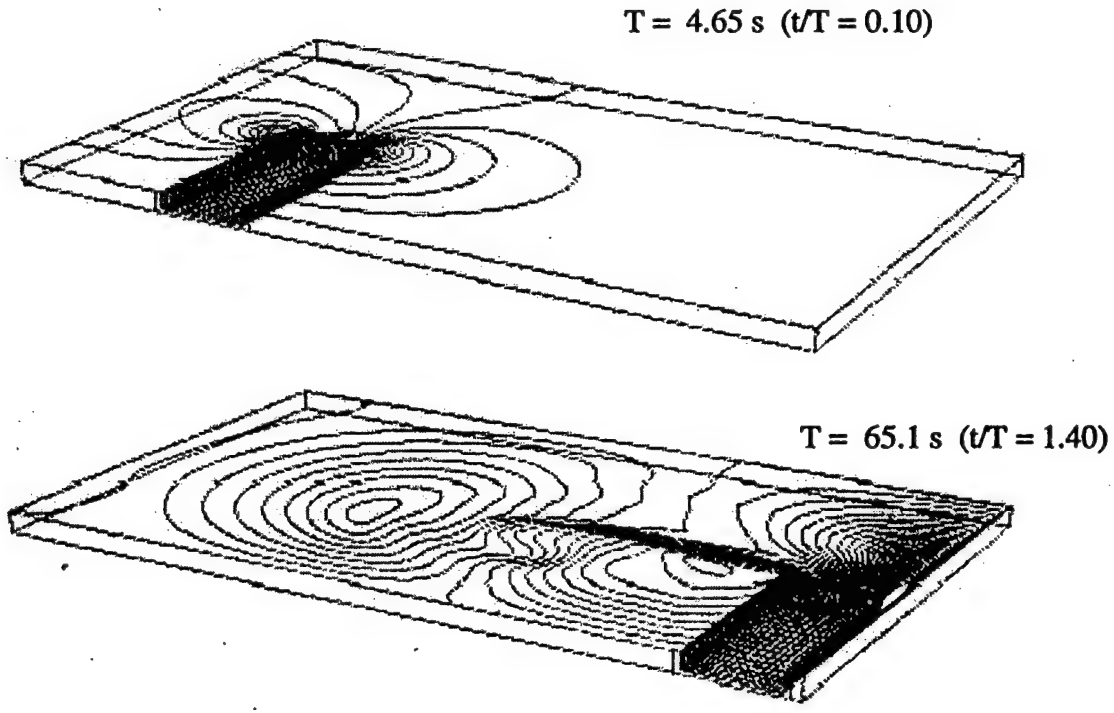

Figure 17. Longitudinal velocity contours.

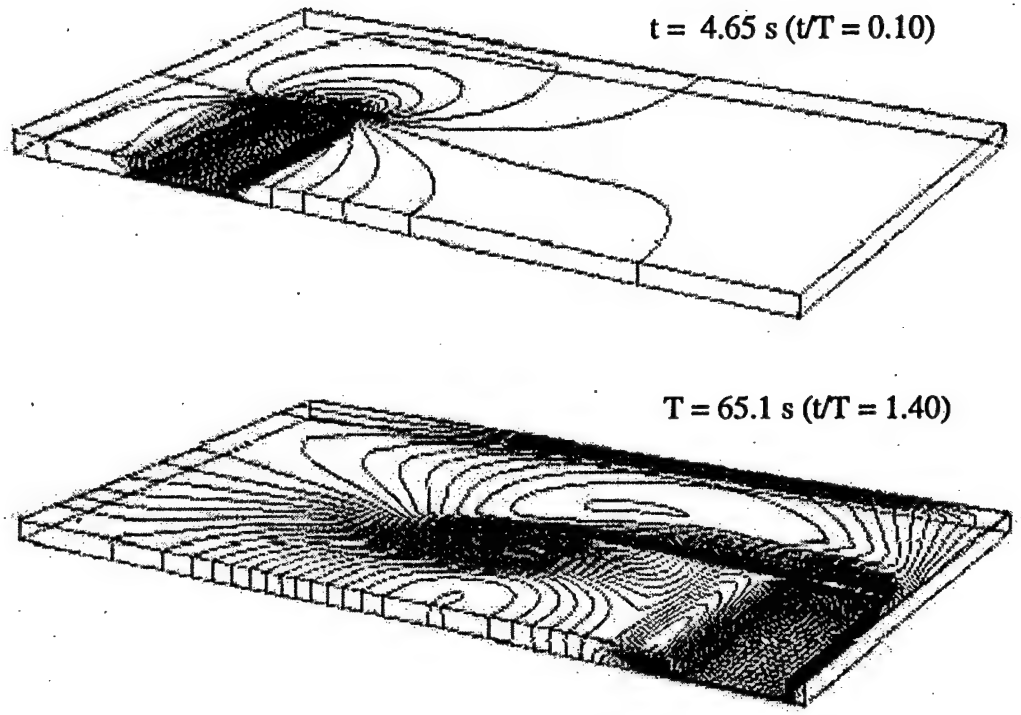

Figure 18. Transverse velocity contours.

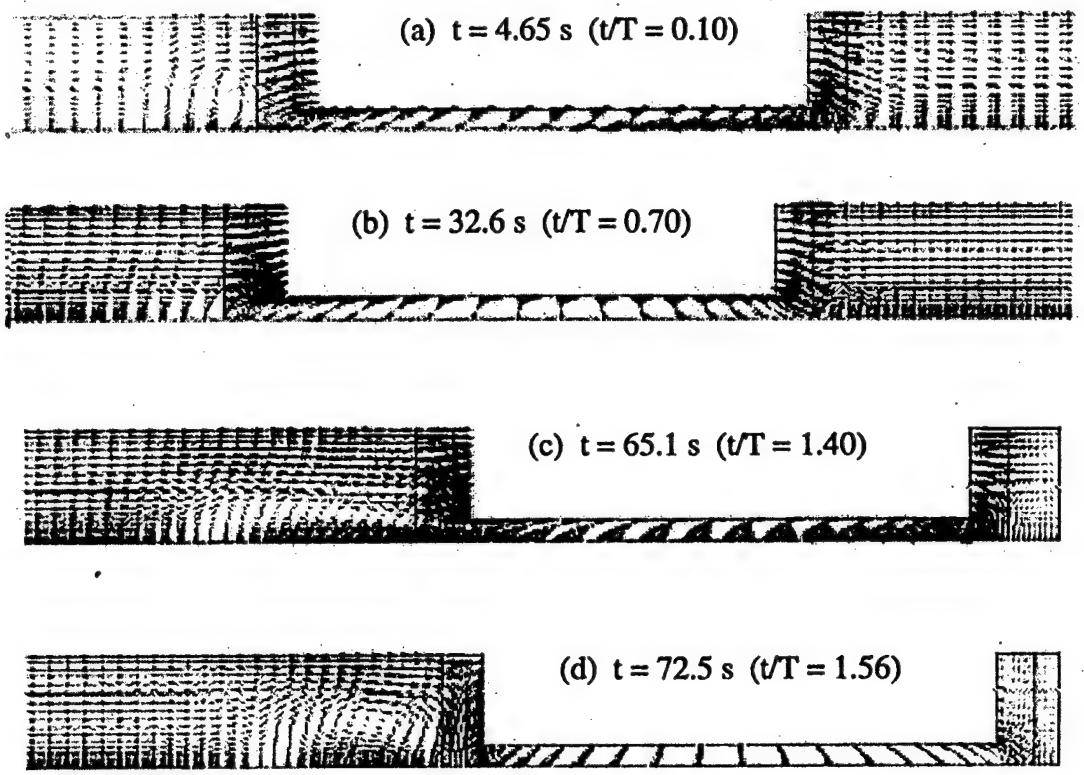

Figure 19. Velocity vectors from simulation model.

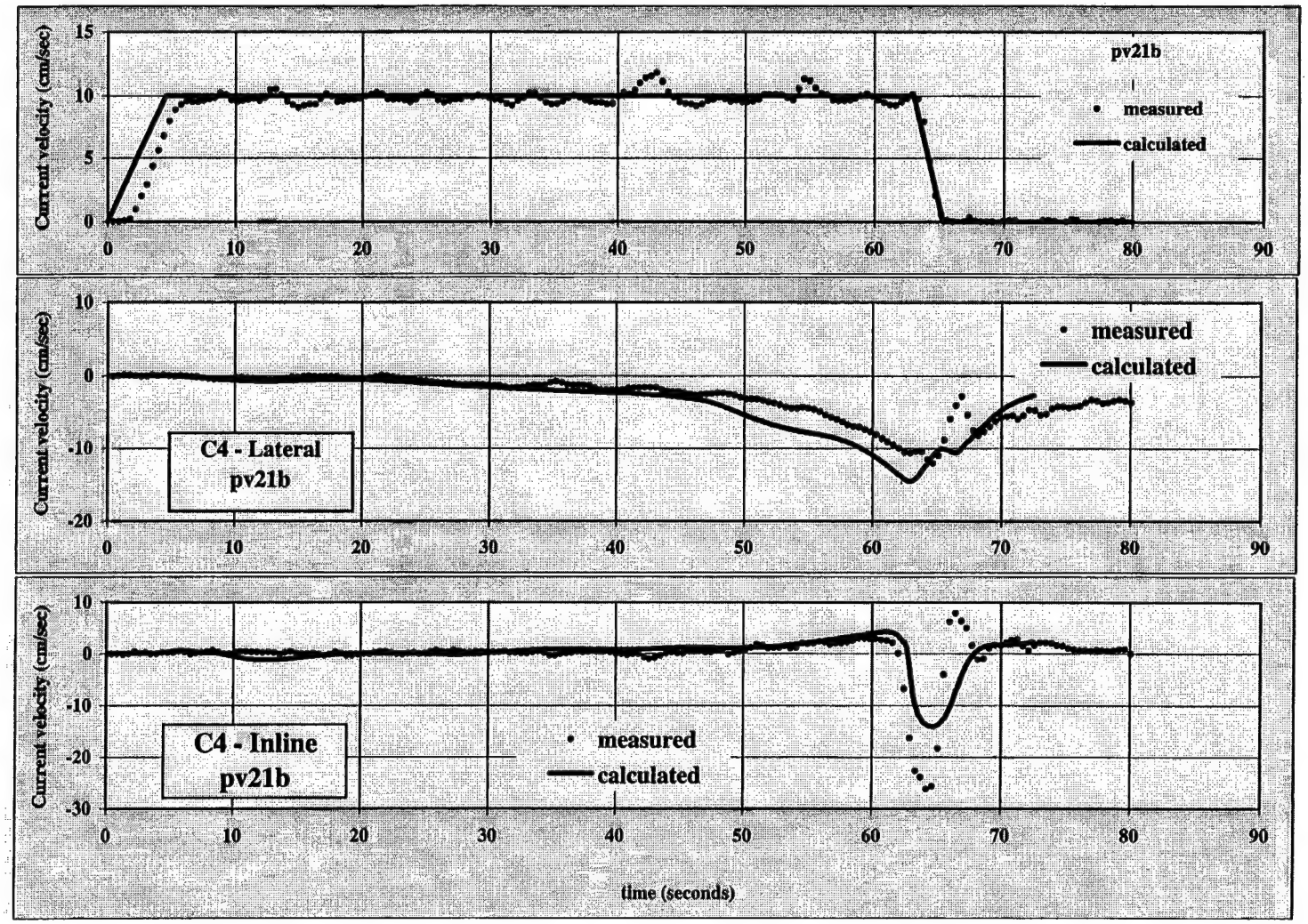

Figure 20. Measured and calculated velocities.

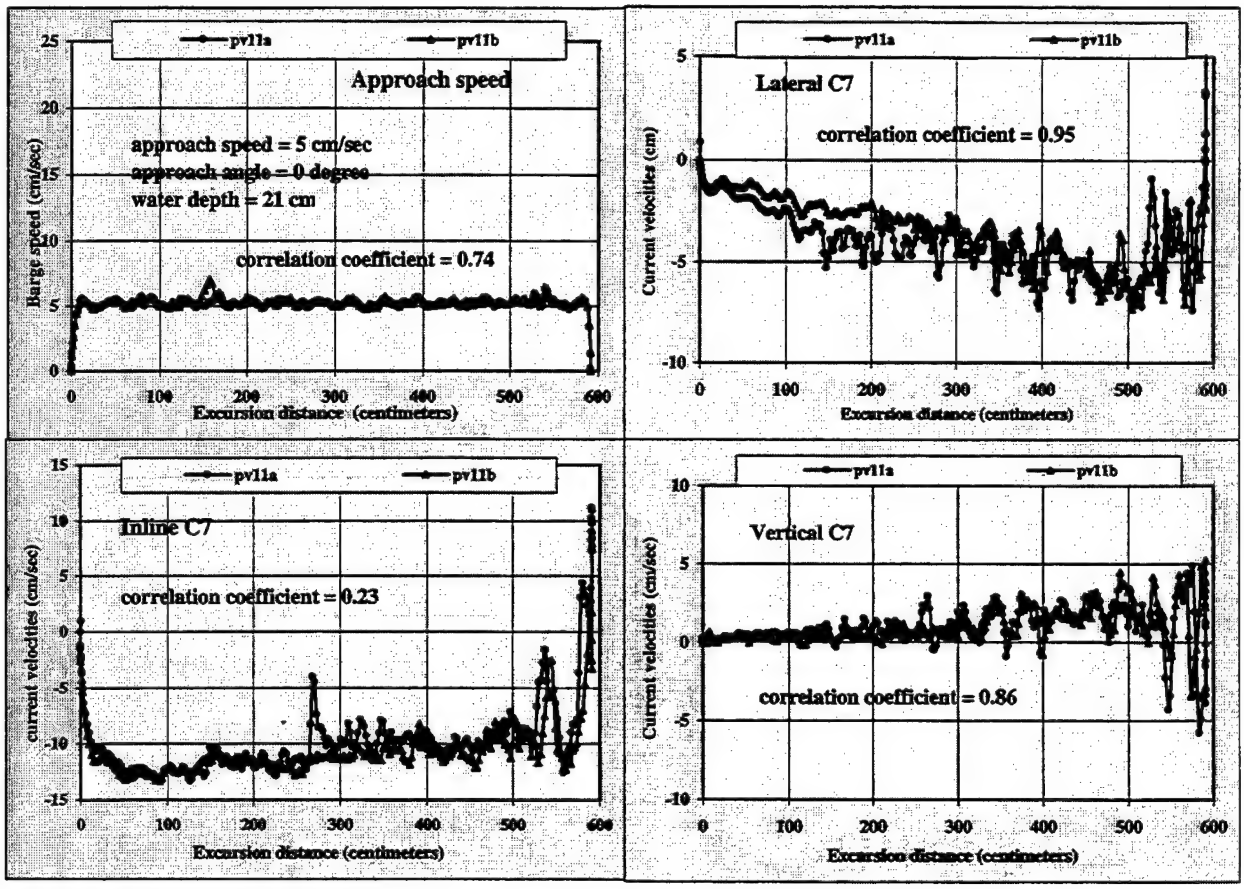

Figure 21. Comparison of velocity measurements at current meter C7 (pv11a and pv11b).

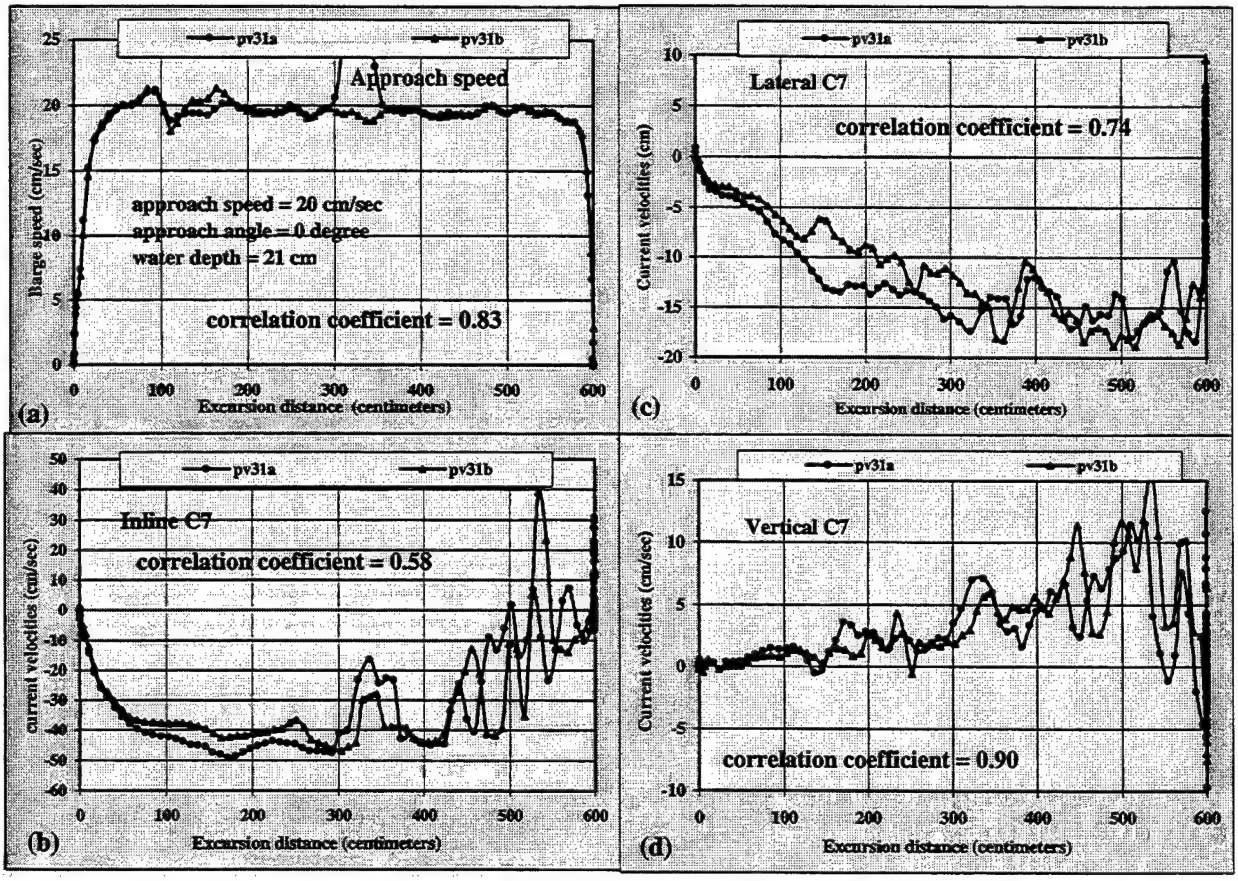

Figure 22. Comparison of velocity measurements at current meter C7 (pv31a and pv31b).

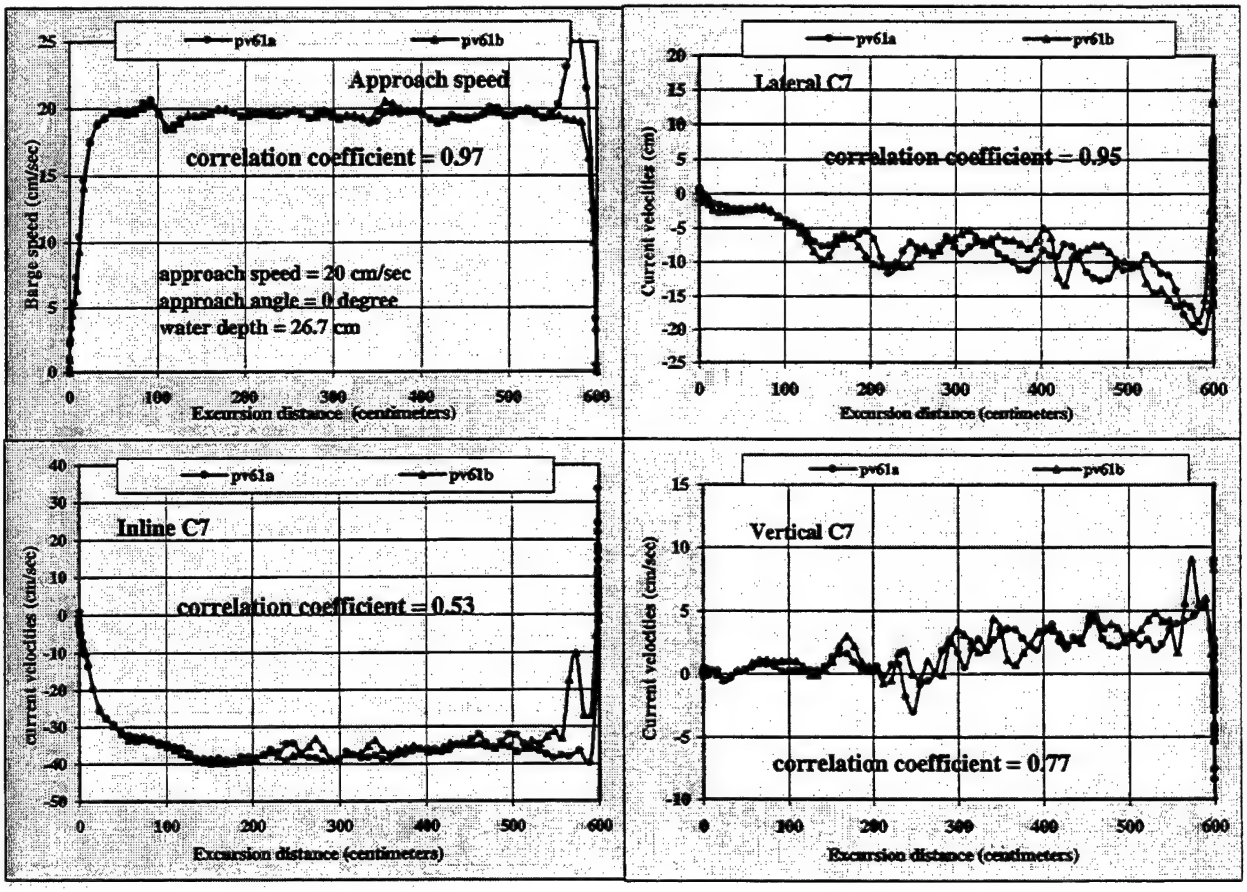

Figure 23. Comparison of velocity measurements at current meter C7 (pv61a and pv61b).

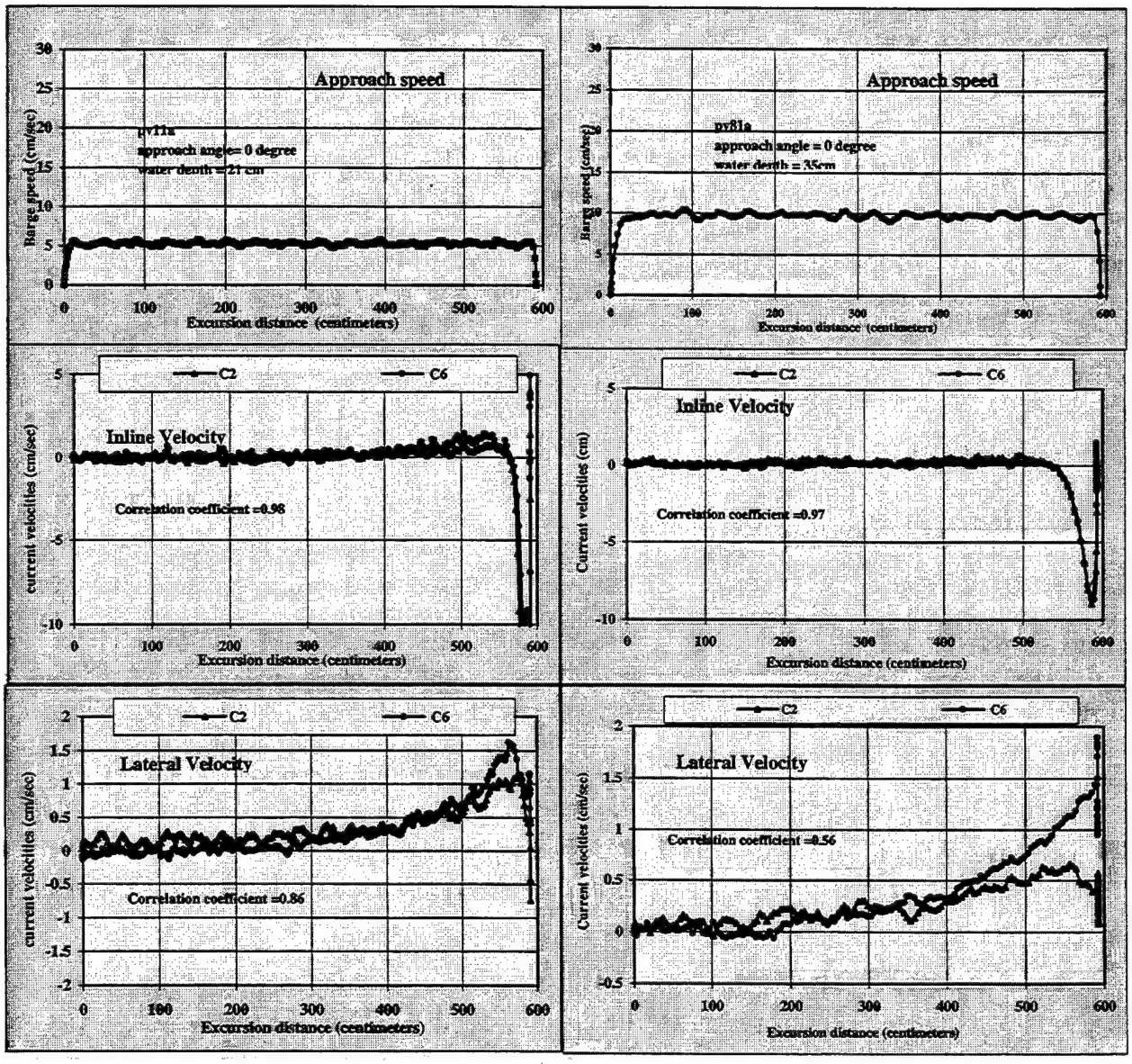

Figure 24. Comparison of velocity measurements at current meters C2 an C6 (pv11a).

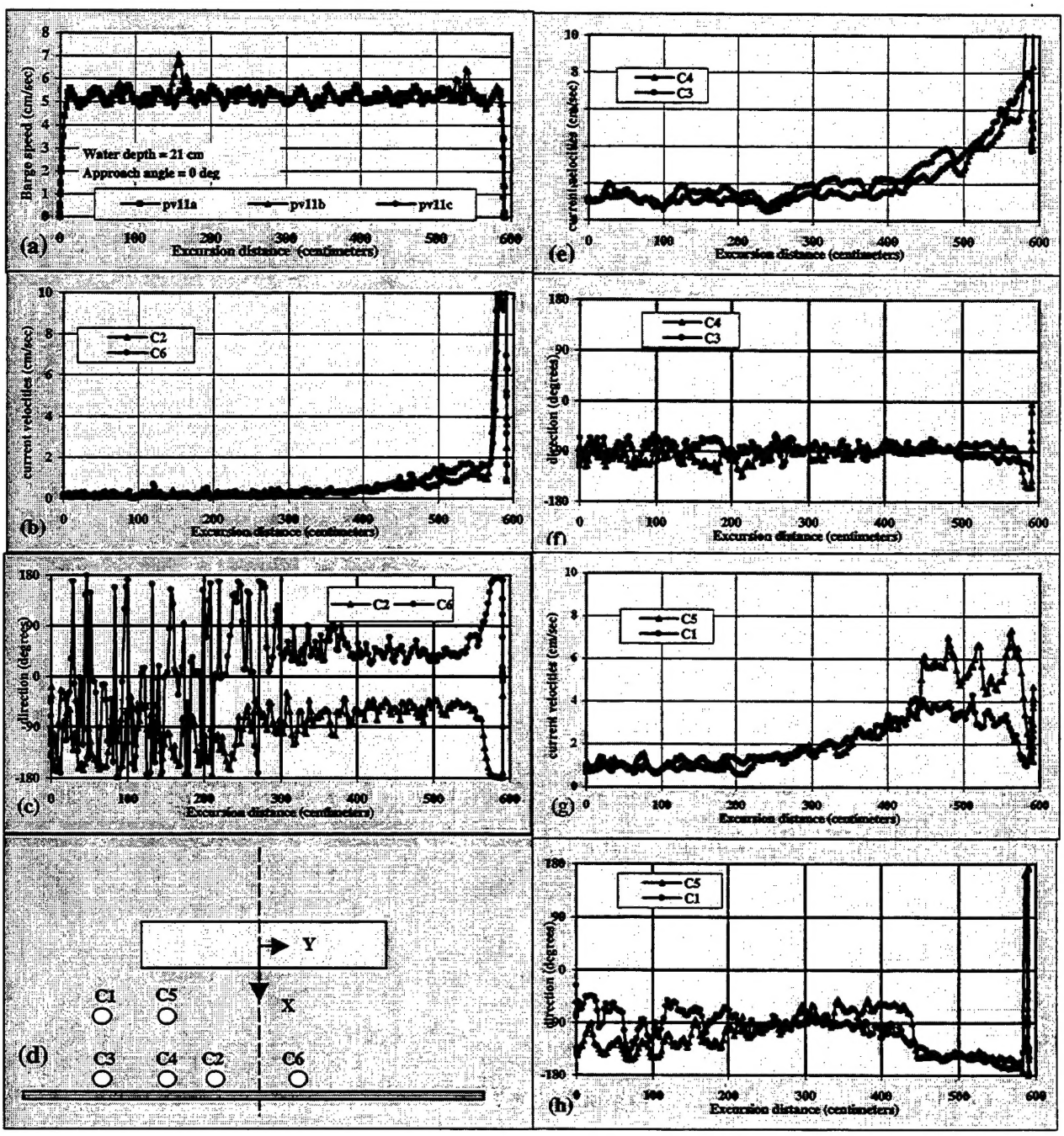

Figure 25. Current measurements at the fixed stations in magnitude and direction.

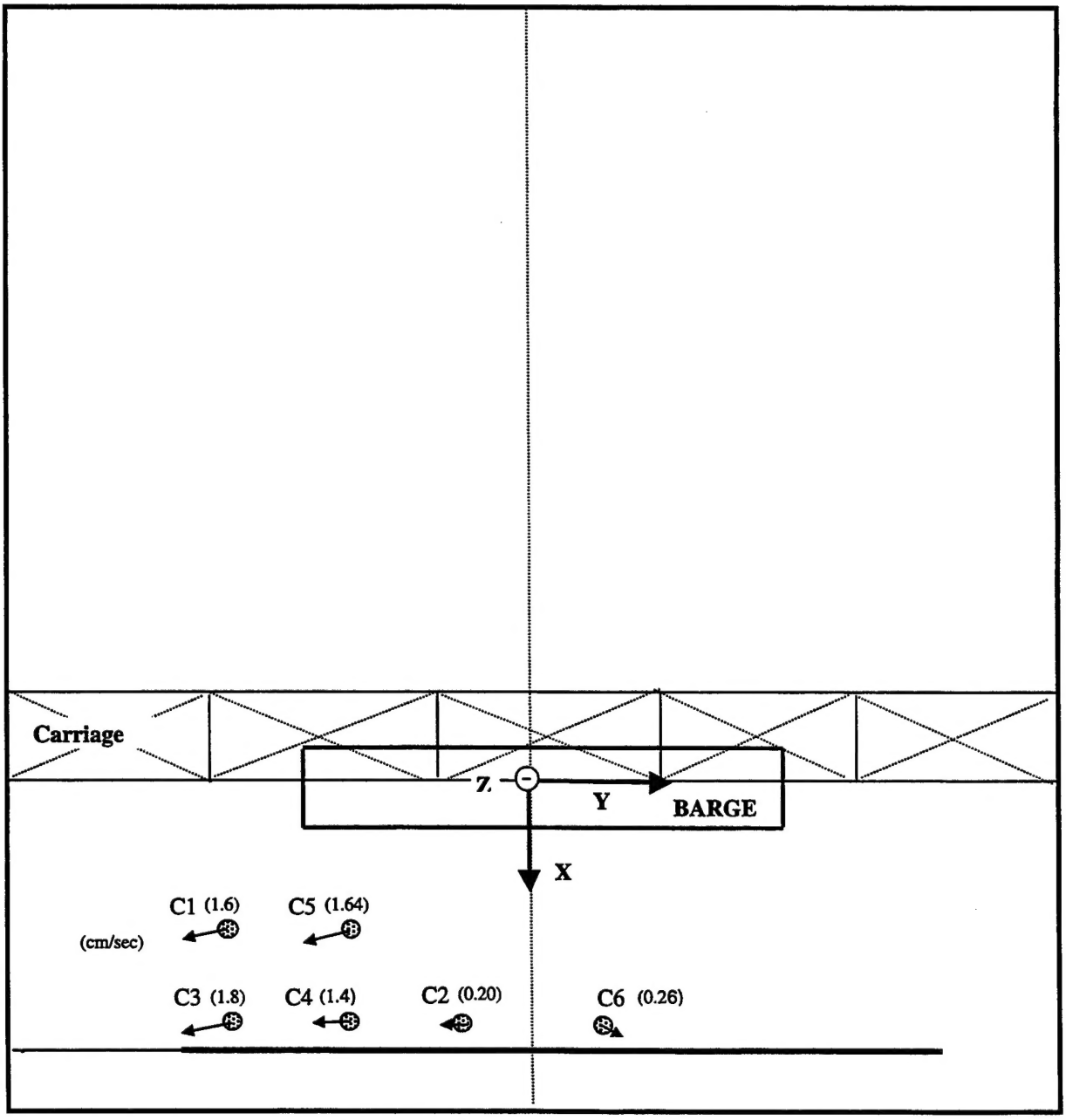

Figure 26. Flow pattern at a barge excursion distance of 300 cm.

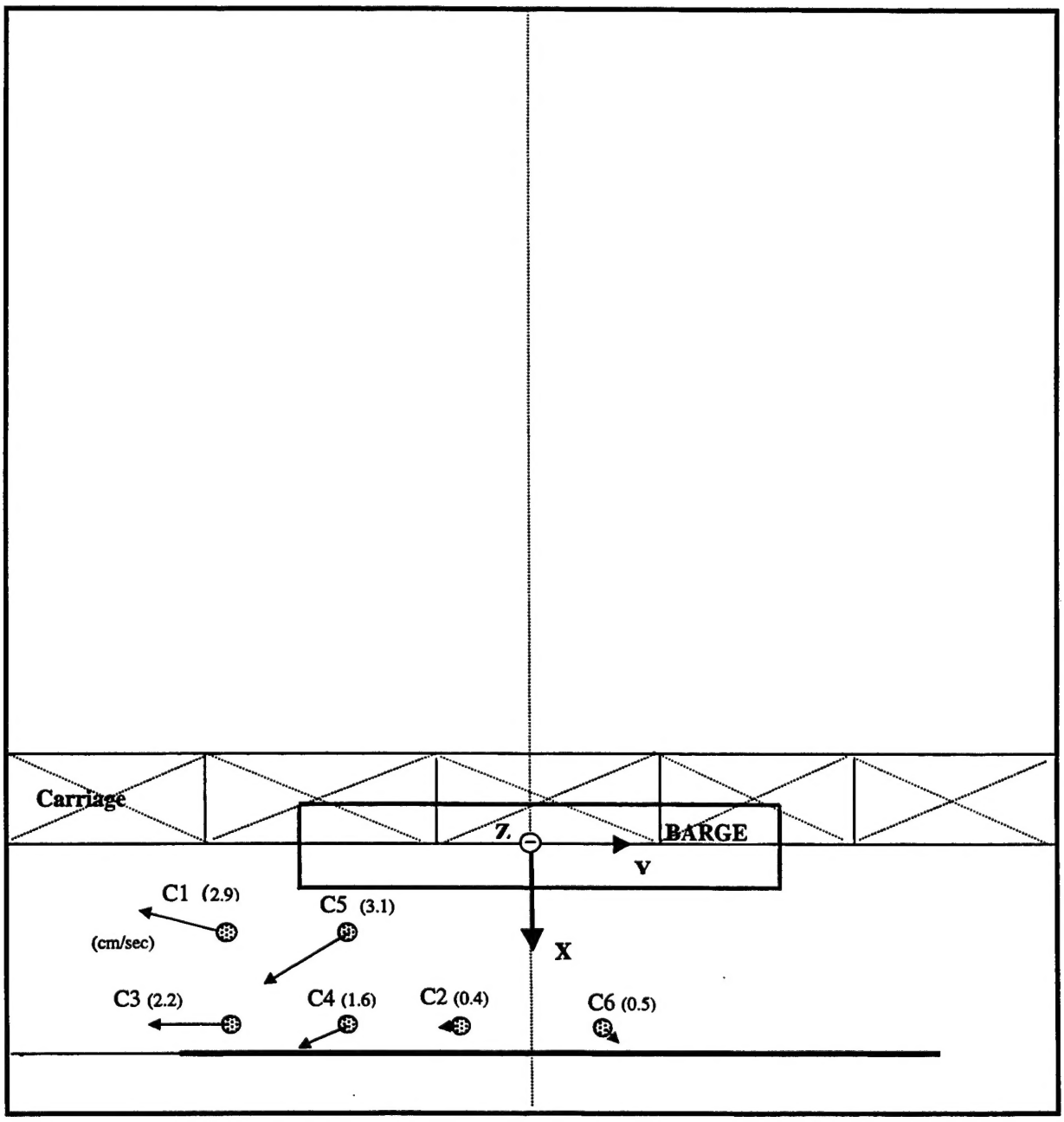

Figure 27. Flow pattern at a barge excursion distance of 400 cm.

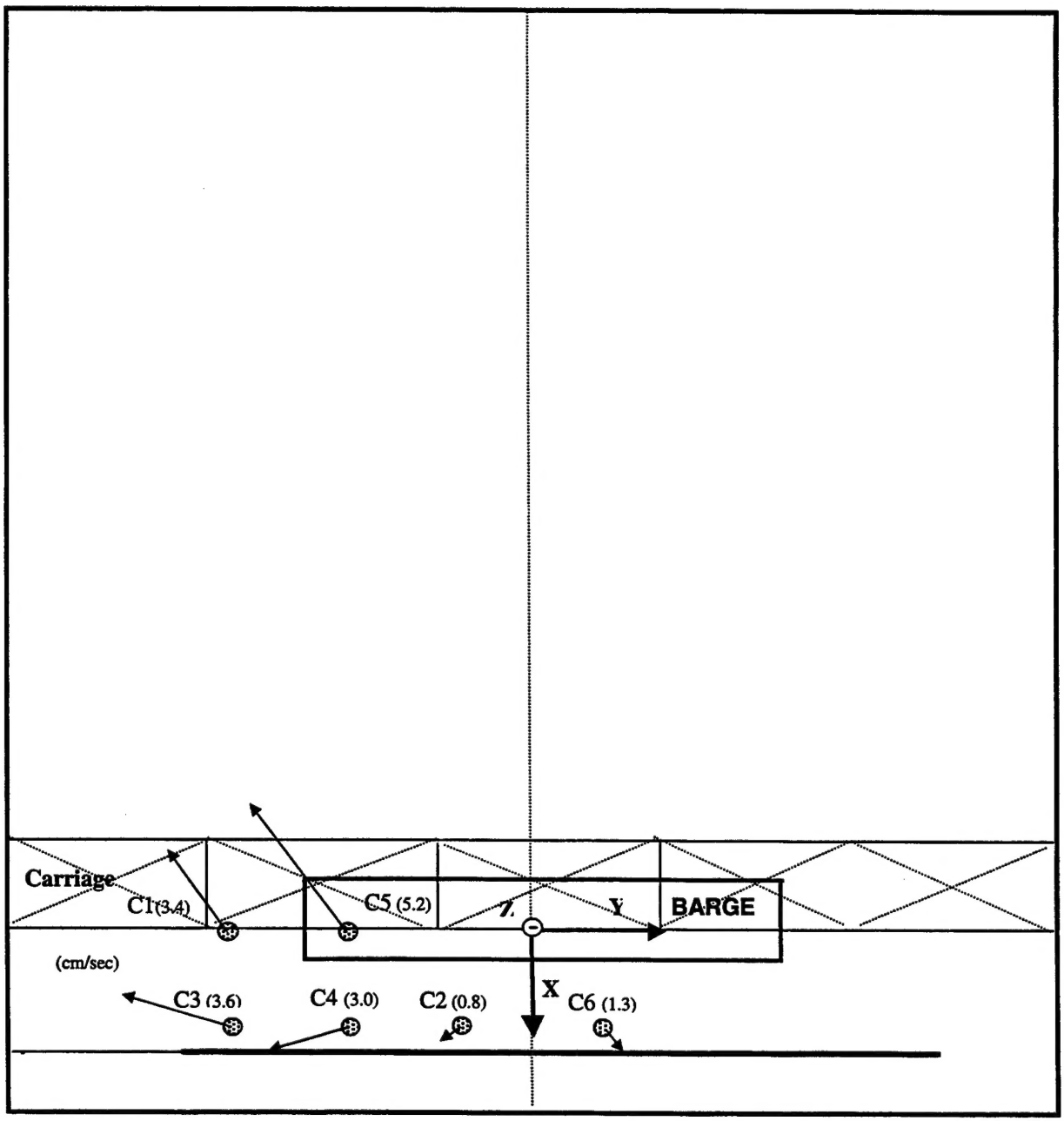

Figure 28. Flow pattern at a barge excursion distance of 500 cm.